Journal Pre-proofs

Renewable bio-based routes to γ-valerolactone in the presence of hafnium nanocrystalline or hierarchical microcrystalline zeotype catalysts

Margarida M. Antunes, Andreia F. Silva, Auguste Fernandes, Martyn Pillinger, Filipa Ribeiro, Anabela A. Valente

PII: S0021-9517(21)00530-3
DOI: https://doi.org/10.1016/j.jcat.2021.12.022
Reference: YJCAT 14452

To appear in: *Journal of Catalysis*

Received Date: 4 October 2021
Revised Date: 22 December 2021
Accepted Date: 23 December 2021

Please cite this article as: M.M. Antunes, A.F. Silva, A. Fernandes, M. Pillinger, F. Ribeiro, A.A. Valente, Renewable bio-based routes to γ-valerolactone in the presence of hafnium nanocrystalline or hierarchical microcrystalline zeotype catalysts, *Journal of Catalysis* (2021), doi: https://doi.org/10.1016/j.jcat.2021.12.022

Renewable bio-based routes to γ-valerolactone in the presence of hafnium nanocrystalline or hierarchical microcrystalline zeotype catalysts

Margarida M. Antunes[a], Andreia F. Silva[a], Auguste Fernandes[b], Martyn Pillinger[a], Filipa Ribeiro[b], Anabela A. Valente[a,*]

[a] *CICECO - Aveiro Institute of Materials, Department of Chemistry, University of Aveiro, Campus Universitário de Santiago, 3810-193 Aveiro, Portugal*

[b] *Centro de Química Estrutural, Instituto Superior Técnico, Universidade de Lisboa, Av. Rovisco Pais, 1049-001 Lisboa, Portugal*

* Corresponding author: atav@ua.pt (A.A. Valente), Tel.: 00351-234-370603

ABSTRACT

Different renewable bio-based routes leading to the versatile bioproduct γ-valerolactone (GVL) were studied in integrated fashions, starting from furfural (Fur), α-angelica lactone (AnL) and levulinic acid (LA), in the presence of multifunctional hafnium-containing catalysts, in alcohol media. These routes involved acid and reduction reactions for which multifunctional catalysts were prepared via top-down strategies, namely the nanocatalyst Hf-deAlBeta-n and the hierarchical (intracrystalline micro/mesopores) microcrystalline material Hf-WdeSAlBeta-m. Mechanistic and kinetic modelling studies, molecular-level investigations by solid-state spectroscopic characterization, and catalyst stability studies led to assessments about the catalytic roles and potentialities of the prepared materials for GVL production. The influences of the catalytic reaction conditions and type of transition metal in the catalysts were studied. The best-performing catalyst was the hierarchical zeotype Hf-WdeSAlBeta-m (GVL yields of up to 99 % from LA, 91 % from AnL, and 73 % from Fur, at 180 ºC), which correlated with its enhanced acidity and mesoporosity.

To the best of our knowledge, this is the first reported hafnium-containing BEA zeotype possessing an intracrystalline hierarchical pore system, and the results highlighted the catalytic potentialities of these types of materials for the integrated production of GVL.

Keywords: heterogeneous catalysis; γ-valerolactone; hafnium; nanocatalysts; hierarchical zeotype

1. Introduction

The considerable dependency of modern industrial society on fossil fuels for power and chemical potential energy, together with stringent environmental legislation and the recognised importance of building a sustainable circular economy, are driving forces in the search for new and/or more efficient industrial production processes [1, 2]. The use of alternative renewable sources of raw materials such as vegetable biomass may make a difference in building a sustainable future [3, 4]. Vegetable biomass is an accessible renewable source of organic carbon, obtainable from non-edible agricultural, forestry, municipal and industrial waste/surpluses or aquatic plants [5, 6].

The main components of vegetable biomass are carbohydrates, which may be converted to a plethora of useful products, contributing to a biobased economy [7-9]. The carbohydrates hemicelluloses and cellulose may be selectively hydrolysed to the monosaccharides D-xylose and D-glucose, respectively, and the latter may undergo consecutive dehydration, giving the respective furanic platform chemicals, furfural (Fur) and 5-(hydroxymethyl)furfural (Hmf). Fur is important in many industrial sectors, including oil refineries (*e.g.*, as a selective solvent in the refining of lubrication oils [10]). The global Fur market is predominantly related to furfuryl alcohol (FA) which is produced via hydrogenation of Fur [11-14]. The broad applications profile of FA includes the production of furan resins (for the foundry industry) [12-16], reactive solvents for the steel industry [12], polymers (*e.g.*, fibre plastics [15-17], polyurethane [12]), agrochemicals [15], pharmaceuticals (*e.g.*, ranitidine) [12, 15] and fragrances [12]. The Fur market may expand as it is being largely explored for producing bio-based fine chemicals, fuels and other commodities [12, 15].

Emerging Fur/FA markets include 2-(alkoxymethyl)furan ethers (AMFs), levulinic acid (LA), alkyl levulinate esters (ALs) and γ-valerolactone (GVL). The reductive etherification of Fur gives AMFs; FA and AMFs may be converted to angelica lactone

isomers (AnLs), LA and ALs; and LA and ALs may be finally converted to GVL [18-22] (Scheme 1). GVL is a relatively stable, low-toxicity [19, 23] and biodegradable [23] renewable chemical, an attractive green solvent, a food flavour and fragrance ingredient, a promising fuel additive [19, 22-26], and an intermediate for producing liquid transportation fuels [23, 24], acrylic monomers [27] and polymers (*e.g.*, Nylon) [19, 24]. In terms of fuel applications, some properties of GVL somewhat parallel those of ethanol, *e.g.*, energy density, low melting point, high boiling and flash points; moreover, GVL advantageously avoids the formation of azeotropic mixtures with water [19, 28]. GVL blended with diesel strategically reduces CO emissions in automobile exhausts [29, 30], and blended with gasoline leads to improved combustion [31].

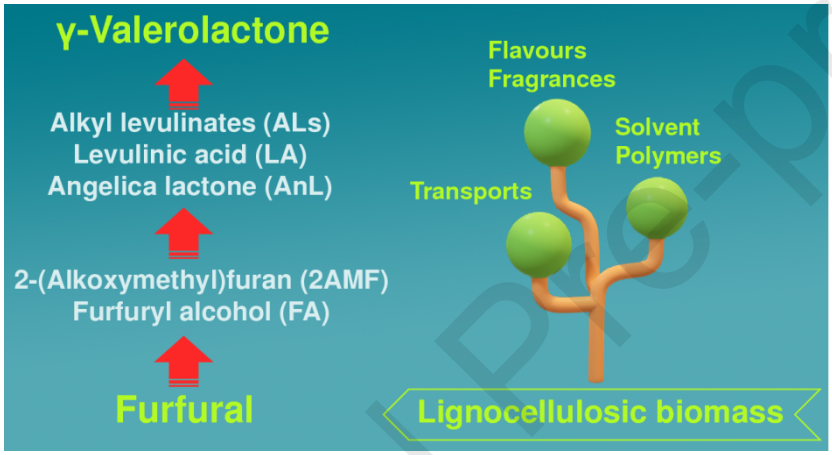

Scheme 1. Conversion of the lignocellulosic biomass-derived platform chemical furfural to the versatile bioproduct γ-valerolactone.

GVL may be synthesised via different renewable bio-based routes. The conversion of LA to GVL is a focus, since LA is in the list of the Top 12 most valuable biomass-derived platform chemicals for the development of a biobased economy [32-34]. Different strategies of LA to GVL production were explored using noble or non-noble metal catalysts and different types of reducing agents (*e.g.*, formic acid, secondary alcohols, molecular hydrogen) [23, 35-37]. The conversion of LA/ALs to GVL without using expensive noble metal catalysts or external H_2 supply (which poses safety and technical issues with respect to H_2 transport, storage and use (especially in high-pressure systems)) is attractive and may be accomplished via catalytic transfer hydrogenation (CTH) involving, for example, a Meerwein-Ponndorf-Verley (MPV) type reaction mechanism [24, 37-41]. The first literature study on the CTH of LA/ALs to GVL was reported by

Dumesic and co-workers [42], using mixed metal oxides containing Zr as catalysts and secondary alcohols as H-donors.

Aiming at process intensification, one-pot heterogeneous catalytic processes for GVL production via acid and CTH reactions were investigated, starting from Fur, FA, D-glucose, D-fructose, sucrose and cellulose and D-xylose [19, 24, 43-47]. Particular attention was given to the integrated conversion of the industrial platform chemical Fur to GVL over non-noble metal zeolite catalysts, most of which possessed zirconium that confers CTH activity; *e.g.*, bulk [20, 46, 48, 49], supported [21, 50, 51], composite [52] or mechanically mixed materials [53, 54]. The material properties may considerably influence the reaction product distributions; *e.g.* differently prepared Sn-containing dealuminated Al-Beta zeolites led to considerably different GVL yields [20, 55]. On the other hand, intrinsic activity for CTH steps may depend on the type of transition metal. A literature survey indicates that Hf-containing catalysts perform superiorly to the Zr or Sn analogues in different bio-based reactions, such as the hydrogenation of Fur and HMF to the respective alcohols FA and 2,5-bis(hydroxymethyl)furan, and the conversion of ALs to GVL [56-59]. To the best of our knowledge, there are only two studies reported in the literature using Hf-based catalysts for the one-pot conversion of Fur to GVL, both of which involved metal-organic frameworks (MOFs): Hf-MOF-808 in conjugation with zeolite Al-Beta [56]; sulfated DUT-67(Hf)-0.06 (for steady catalytic performance in consecutive batch runs, the used catalyst was sulfated again with H_2SO_4 as in the post-synthetic modification step) [60].

In the present study, different integrated bio-based routes leading to GVL were investigated, starting from Fur, AnL and LA, and using hafnium-containing multifunctional zeotype catalysts, in alcohol media. Commercially available nanocrystalline and microcrystalline Beta zeolites were modified via top-down strategies leading to the nanocatalyst Hf-deAlBeta-n and the hierarchical microcrystalline catalyst Hf-WdeSAlBeta-m (possessing intracrystalline micro/mesopores, *i.e.*, which make part of the crystal). A zirconium counterpart of Hf-deAlBeta-n was prepared in an identical fashion for comparison studies. The Hf-containing catalysts led to higher GVL yields than the zirconium catalyst. The influence of the reaction temperature and type of alcohol H-donor agent was investigated. Mechanistic and kinetic modelling studies, molecular-level investigations by solid-state spectroscopic characterization, and detailed stability studies (based on catalytic tests and characterization of the used solids) led to assessments about the catalytic roles and potentials of the Hf-catalysts. To the best of our knowledge,

this is the first report on the synthesis of a hafnium-containing BEA zeotype possessing an intracrystalline hierarchical pore system.

2. Experimental

The specifications of the materials used are given in the Supplementary Material.

2.1. Preparation of the materials

Hafnium-containing Beta zeotypes and a Zr-counterpart were prepared via post-synthesis modifications, which were adapted from the literature for other materials [55, 61, 62]. Specifically, dealumination (deAl) was carried out for the parent nanocrystalline (n) zeolite H-Beta-n, and, on the other hand, dealumination/desilication/acid-wash (WdeSAl) were carried out for the parent microcrystalline (m) zeolite H-Beta-m. The aluminosilicates deAlBeta-n and WdeSAlBeta-m were subjected to solid-state impregnation (SSI) of a transition metal (M = Hf, Zr) precursor, followed by calcination, to give M-deAlBeta-n (M = Hf, Zr) and Hf-WdeSAlBeta-m, respectively. The molar amount of M per mass unit of aluminosilicate was constant for all M-containing materials prepared.

The alkaline treatment may allow mesopores to be "carved" on the zeolite Beta crystal, and the formation of the mesopores may develop from the outer surface towards the inner surface of the crystal; *e.g.* if the pore walls between adjacent 12-membered rings are partially destroyed, enlarged pores may be formed (mesopores), while other 12-membered rings (micropores) may be preserved in the vicinity of those enlarged pores. To the best of our knowledge, this is the first report of a hafnium-containing BEA zeotype possessing an intracrystalline hierarchical pore system (Hf-WdeSAlBeta-m). Wang *et al.* [63] reported Hf-Beta zeolites which were ion-exchanged using aqueous NaOH and subsequently washed using H_2SO_4; the base and acid treatments did not affect the microporous volume (0.19 - 0.20 $cm^3\ g^{-1}$) and there was no indication of mesoporosity, and the N_2 sorption isotherms were always of Type I, characteristic of microporous zeolites.

2.1.1. Aluminosilicate zeotypes

Nanocrystalline zeolite H-Beta-n was dealuminated (deAl) using 13 M HNO_3 (20 mL per gram of zeolite) at 100 ºC during 20 h, under stirring. The solid was separated by

filtration, thoroughly washed with hot Milli-Q water until neutral pH, and dried overnight at 65 °C, giving deAlBeta-n.

Microcrystalline zeolite H-Beta-m was mildly dealuminated (deAl), using 0.03 M aq. oxalic acid (20 mL per gram of zeolite) at 70 °C during 3 h, with stirring; this pre-procedure may introduce surface defect sites and facilitate the subsequent desilication process to form intracrystalline mesopores [64]. The solid was separated by filtration, thoroughly washed with hot Milli-Q water until neutral pH, dried overnight at 100 °C and finally calcined at 550 °C (1 °C min^{-1}) in static air during 5 h, giving deAlBeta-m. Subsequently, deAlBeta-m was desilicated using 0.2 M NaOH (20 mL per gram of zeolite) at 65 °C for 30 min, with stirring. The solid was separated by filtration, thoroughly washed with hot Milli-Q water until neutral pH and dried overnight at 100 °C, giving deSAlBeta-m. The desilicated material deSAlBeta-m was treated with 13 M HNO_3 (20 mL per gram of zeolite) at 100 °C during 20 h, with stirring; this treatment may simultaneously exchange sodium cations for hydronium ions and wash-out (W) inorganic debris formed during the desilication step. The resultant solid was separated by filtration, thoroughly washed with hot Milli-Q water until neutral pH, and dried overnight at 65 °C, giving the washed (W) material WdeSAlBeta-m. For comparison, the same protocol was used for preparing deAlBeta-n, was applied to H-Beta-m, giving deAl(HNO_3)Beta-m (a dealuminated, non-desilicated counterpart).

2.1.2. M-containing materials

The materials deAlBeta-n (derived from H-Beta-n) and WdeSAlBeta-m (derived from H-Beta-m) were subjected to SSI with M$(acac)_4$ where M = Zr, Hf (0.274 mmol of M per gram of aluminosilicate) and calcination, giving M-deAlBeta-n and Hf-WdeSAlBeta-m, respectively. Specifically, 1 g of deAlBeta-n or 1 g of WdeSAlBeta-m was mixed with Hf$(acac)_4$ (0.274 mmol, 0.157 g) and gently ground using an agate pestle and mortar, during 30 min, followed by calcination at 550 °C (1°C min^{-1}) under air flow (20 mL min^{-1}) during 6 h, giving Hf-deAlBeta-n and Hf-WdeSAlBeta-m, respectively (4.8 wt% Hf). The same protocol was used for preparing Zr-deAlBeta-n (2.4 wt% Zr), using Zr$(acac)_4$ (0.274 mmol, 0.134 g) instead of Hf $(acac)_4$. For comparison, the SSI/calcination protocol was applied directly to commercial H-Beta-m, deAl(HNO_3)Beta-m and ordered mesoporous silica MCM-41 (synthesis described in the Supplementary Material), which gave Hf-Beta-m, Hf-deAl(HNO_3)Beta-m and Hf-MCM-41, respectively.

2.2. Characterization of the materials

The X-ray powder diffraction (PXRD) data were collected on an Empyrean PANalytical diffractometer (Cu-Kα X-radiation, λ = 1.54060 Å) in a Bragg-Brentano *para*-focusing optics configuration (45 kV, 40 mA) at ambient temperature. Samples were prepared in a spinning flat plate sample holder and step-scanned in the range from 3° to 68° (2θ) with steps of 0.026°. A PIXEL linear detector with an active area of 1.7462° was used with a scan speed of 0.0515° per second. Scanning electron microscopy (SEM) images and elemental mappings (Zr, Hf, Si, Al) were obtained on a Hitachi SU-70 SEM microscope with a Bruker Quantax 400 detector operating at 20 kV.

Nitrogen adsorption-desorption isotherms were measured at -196 °C, using a Quantachrome instrument (automated gas sorption data using Autosorb IQ_2). The samples were pre-treated at 250 °C for 3 h, under vacuum (< 4×10^{-3} bar). The specific surface area was calculated using the Brunauer, Emmett, Teller equation (S_{BET}) and the total pore volume (V_p) was determined by using the Gurvitsch rule (for relative pressure (p/p_0) of at least 0.993). The external/mesoporous surface area (S_{EM}) and mesoporous volume (V_M) were calculated using the t-plot method. The pore size distributions were determined by the DFT method (adsorption branch).

Cross polarization (CP) $^{29}Si\{^1H\}$ CP MAS NMR spectra were acquired at 79.495 MHz on a Bruker Avance III 400 MHz (9.4 T magnetic field) spectrometer, using a 7 mm double-bearing probe with 3.5 μs ^1H 90º pulses, 8000 μs contact time, a 5 s recycle delay and a spinning rate of 5 kHz. The chemical shifts are quoted in ppm from tetramethylsilane (TMS). Diffuse reflectance UV–vis spectra were recorded on a GBC Cintra 303 spectrophotometer using an integrating sphere (MgO) with light detection by a built-in photomultiplier tube attached to the base of sphere, in reflectance mode with a wavelength scan speed of 100 nm min^{-1} in the range 200 to 800 nm, step size of 0.520 nm, and a slit width of 5.0 nm. X-ray photoelectron spectroscopy (XPS) analysis was performed using an Ultra High Vacuum (UHV) system (high-resolution electron energy analyzer; standard spot size of 2 mm) with a working pressure of 2×10^{-10} mbar, located at TEMA, University of Aveiro. The system is equipped with a hemispherical electron energy analyzer (SPECS Phoibos 150), a delay-line detector and a monochromatic Al-K_α X-ray source (1486.74 eV). High resolution spectra were recorded at normal emission take-off angle and with a pass energy of 20 eV, which provides an overall instrumental

peak broadening of 0.5 eV. Binding energies of all spectra were recalibrated with respect to the carbon position by shifting the C 1s line (adventitious carbon) to 284.8 eV.

The acid properties were measured using a NexusThermo Nicolet apparatus (64 scans and resolution of 4 cm^{-1}) equipped with a specially designed cell, using self-supported discs (5–10 mg cm^{-2}) and pyridine as base probe. After *in situ* outgassing at 450 ºC for 3 h under vacuum (10^{-6} mbar), pyridine (99.99 %) was contacted with the sample at 150 ºC for 10 min, and subsequently evacuated at 150 ºC or 350 ºC for 30 min, under vacuum. The quantitative measurements were based on the integration of IR bands at *ca.* 1540 and 1455 cm^{-1} which are associated with pyridine adsorbed on Brønsted (B) and Lewis (L) acid sites, respectively, and using extinction molar coefficients from Emeis [65].

For temperature programmed desorption of NH_3 (NH_3-TPD), the sample was pre-treated at 350 °C (10 °C min^{-1}) for 1 h, under He flow (30 mL min^{-1}), and then cooled to 125 ºC and saturated with NH_3 (15 % NH_3 in He) for 1 h. Afterwards, the samplewas purged with He for 1 h and then heated until 750 °C (10 °C min^{-1}). Desorbed NH_3 was analysed using thermal conductivity detector (TCD) and quantified via deconvolution/peak integration of the NH_3-TPD curves in the range 200-400 °C (this range was chosen to avoid overlapping signals due to *e.g.* desorption of structural water molecules).

The composition of the samples was measured by Inductively-Coupled Plasma Optical Emission Spectrometry (ICP-OES) using a Perkin Elmer 2000 DV equipment (for Al, Hf, Zr), and Flame Atomic Absorption (AA) using a Perkin Elmer PinAAcle 500 spectrometer (for Si); all samples were digested using HNO_3 and HF (experimental range of error of *ca.* 10 %). Elemental analysis for C of the used catalysts were obtained using a Leco TruSpec 630-200-200 analyzer. Thermal analyses were performed on a Setsys Evo 15 thermobalance (Setaram), at a heating rate of 10 ºC min^{-1} from room temperature to 800 °C, under air.

2.3. Catalytic tests

The catalytic reactions were carried out using (partly homemade) tubular borosilicate batch reactors (*ca.* 8 cm length, *ca.* 11 mm internal diameter, 1.5 mm wall thickness) with a conical shaped bottom, equipped with a PTFE-coated magnetic stirring bar (Supelco) and a PTFE valve (Normax) for purging. Each reactor was loaded with 26.7 $g_{catalyst}$ L^{-1} and a solution of 0.45 M substrate in a secondary alcohol (2-butanol or 2-propanol); the substrates were furfural (Fur), α-angelica lactone (AnL) and levulinic acid (LA). The

reactors (*ca.* 1 mL volume of reaction mixture) were immersed in a thermostatically controlled oil bath heated at 150 or 180 °C (autogenous pressure) and stirred at 1000 rpm for a uniform temperature distribution and to avoid external diffusion limitations. Reaction time was counted from the instant the reactor was immersed in the oil bath. Blank tests without catalyst were performed for each substrate at 150 and 180 °C.

At a given reaction time, the reactors were cooled to room temperature prior to sampling. Freshly prepared samples were analysed by gas chromatography (GC) for quantification of the reaction products (including 2-*sec*-butoxybutane formed from 2-butanol) and substrates, excluding Fur which was analysed by high performance liquid chromatography (HPLC). The GC analyses were carried out using an Agilent 7820A GC equipped with a capillary column (HP-5, 30 m × 0.320 mm × 0.25 mm) and a flame ionization detector. The HPLC analyses were carried out using a Knauer Smartline HPLC Pump 100 and Shodex SH1011 H+ 300 mm × 8 mm (i.d.) ion exchange column (Showa Denko America, Inc. New York), coupled to a Knauer Smartline UV detector 2520 (254 nm). The mobile phase was 0.005 M aq. H_2SO_4 at a flow rate of 0.8 mL min^{-1} and the column temperature was 50 °C. Calibration curves with internal standards were measured for the quantification of the substrates and reaction products. Individual experiments were performed for a given reaction time and the presented results are the mean values of at least two replicates (error < 5 %). The reaction products were identified using a Shimadzu QP2010 ultra-GC-MS (Izasa Scientific, Lisbon, Portugal) equipped with a Zebron ZB-5MS capillary GC column (ZB-5, 30 m × 0.25 μm × 0.25 mm) and He as carrier gas (supporting databases: Wiley229 and NIST14). The quantified products were furfuryl alcohol (FA), 2-(alkoxymethyl)furan ethers (AMFs; 2-(*sec*-butoxymethyl)furan (2BMF) or 2-(isopropoxymethyl)furan (2PrMF), levulinate esters (2-butyl levulinate (2BL) or 2-propyl levulinate (2PrL)), angelica lactone isomers (AnLs = β-angelica lactone + α-angelica lactone) and γ-valerolactone (GVL). The conversion (%) of the substrate (Sub) at a reaction time *t* was calculated using the formula, 100 × [(initial molar concentration of Sub) - (molar concentration of Sub at reaction time t)/(initial molar concentration of Sub)], and product (Prod) yield was calculated using the formula 100 × [(molar concentration of Prod at time t)/(initial molar concentration of Sub)]. Initial activities (mmol g_{cat}^{-1} h^{-1}) and turnover frequencies (TOF expressed as mol mol_M^{-1} h^{-1}) were calculated based on conversion at 1 h reaction. The carbon molar balances were calculated considering the quantified products (listed above) and the amount of unreacted substrate.

The used catalysts were separated by centrifugation at 10000 rpm, thoroughly washed with the same solvent that was used in the catalytic reaction (2-butanol or 2-propanol) and dried at 85 °C overnight; the solids were brownish in colour due to the presence of carbonaceous matter (checked by thermal (Fig. S13) and elemental analyses). The organic matter was removed from the catalysts by calcination at 550 °C (heating rate of 1 °C min^{-1}) for 5 h, under air flow of 20 mL min^{-1} (leading to white solids). The stability studies involved catalyst reuse for up to four consecutive 24 h-batch runs (Fur reaction, using 2-butanol at 180 °C), contact tests and characterization of the recovered Hf-containing materials. The contact tests (CT) consisted of contacting the fresh catalysts with 2-butanol at 180 °C for 24 h under the same conditions as those used for a normal catalytic test, but without substrate; after separating the solid by centrifugation (10000 rpm), the liquid phase was passed through a 220 nm pore size PTFE membrane; subsequently, the substrate (Fur) was added to the obtained permeate (to give an initial substrate concentration of 0.45 M); finally, the homogeneous phase reaction was monitored for 24 h at 180 °C.

Based on the reaction mechanism given in Scheme 2, a pseudo-homogeneous kinetic model was developed, which is described in detail in the Supplementary Material.

3. Results and Discussion

3.1. Characterization of the materials

Nanocrystalline and hierarchical microcrystalline hafnium-containing BEA type materials were prepared via top-down strategies, and a zirconium analogue was prepared for comparison. Framework Al and/or Si atoms of commercial Beta zeolites were partially removed via dealumination (for nanocrystalline H-Beta-n with Si/Al of *ca.* 12) or dealumination/desilication/acid-wash (for microcrystalline H-Beta-m with Si/Al = 14, Table 1), leading to framework vacant sites [55, 61, 62]. The dealuminated materials deAlBeta-n, (desilicated (deS)) WdeSAlBeta-m and (non-desilicated) deAl(HNO_3)Beta-m possessed a much higher Si/Al ratio (510, 697 and 763, respectively) than the respective commercial zeolites. These materials were subsequently subjected to solid-state impregnation (SSI) and calcination of a transition metal precursor, giving M-deAlBeta-n (M = Zr, Hf), Hf-WdeSAlBeta-m and Hf-deAl(HNO_3)Beta-m with Si/M molar ratio in the range 43-51 measured by ICP and AA (Table 1). The M-containing zeolitic materials possessed similar concentration of M sites (0.27-0.29 $mmol_M$ g^{-1}),

consistent with the calculated amount of $M(acac)_2$ added in the SSI procedure (0.274 $mmol_M$ g^{-1}). The calculated value of *ca.* 0.274 mmol M per gram of hydrated zeolite precursor corresponds to *ca*. 0.306-0.323 mmol M per gram of dehydrated precursor (mass basis corrected, based on TGA of the precursors) and estimated Si/M molar ratios of *ca.* 51-54; these ratios are slightly higher than the experimental values (43-51), which may be partly due to experimental errors (*e.g.*, associated with the SSI protocol, sample pre-treatments (digestion/dilutions) prior to bulk elemental analyses).

Table 1. Composition[a] and acid properties[b] of the M-containing zeotypes (M = Hf, Zr).

Sample	Si/Al	Si/M	M[a] (mmol g^{-1})	L (µmol g^{-1})	B (µmol g^{-1})	L+B[b] (µmol g^{-1})
H-Beta-n	12	-	-	199	152	351
deAlBeta-n	510	-	-	0	7	7
Hf-deAlBeta-n	495	43	0.28	73	20	93
Zr-deAlBeta-n	506	47	0.27	42	4	46
H-Beta-m	14	-	-	344	268	612
Hf-Beta-m	14	43	0.28	323	195	518
WdeSAlBeta-m	697	-	-	0	0	0
Hf-WdeSAlBeta-m	698	44	0.29	95	15	110
Hf-deAl(HNO_3)Beta-m	749	51	0.27	60	10	70

[a] Measured by ICP and AA. [b] Measured by FT-IR spectroscopy of adsorbed pyridine (150 °C): L = Lewis acid sites; B = Brønsted acid sites.

The BEA topology of the parent commercial zeolites (H-Beta-n, H-Beta-m) was confirmed by PXRD (Fig. 1). All prepared Beta type materials exhibited reflections characteristic of this topology (main peaks at *ca.* 7.5–8 and 22.4° 2θ [66]), indicating that the materials retained the BEA structure during the post-synthesis modification. However, the reduction of the intensities of the peaks for the modified materials suggests partial loss of crystallinity. The M-containing Beta type materials (Fig. 1 and Fig. S1) did not exhibit reflections associated with crystalline hafnia (*e.g.* peaks at 28.6°, 31.8° and 34.7° for the monoclinic phase (ICDD PDF-4+ 2020 reference code no. 04-005-4477)) or zirconia (e.g. peaks at 28.2° and 31.5° for the monoclinic phase (ICDD PDF-4+ 2020

reference code no. 04-015-4188)) [67]. These results suggest that the materials possessed relatively uniform M-distributions.

The SEM images showed relatively good preservation of the morphology during the post-synthesis modifications (Fig. 2 and Fig. S1A,D); specifically, the nanomaterials consisted of nanoparticles and the microcrystalline materials consisted of particles with sizes in the range 200-500 nm. The element mappings showed uniform distributions of Si, Al and M (Figs. S1C, S2 and S3).

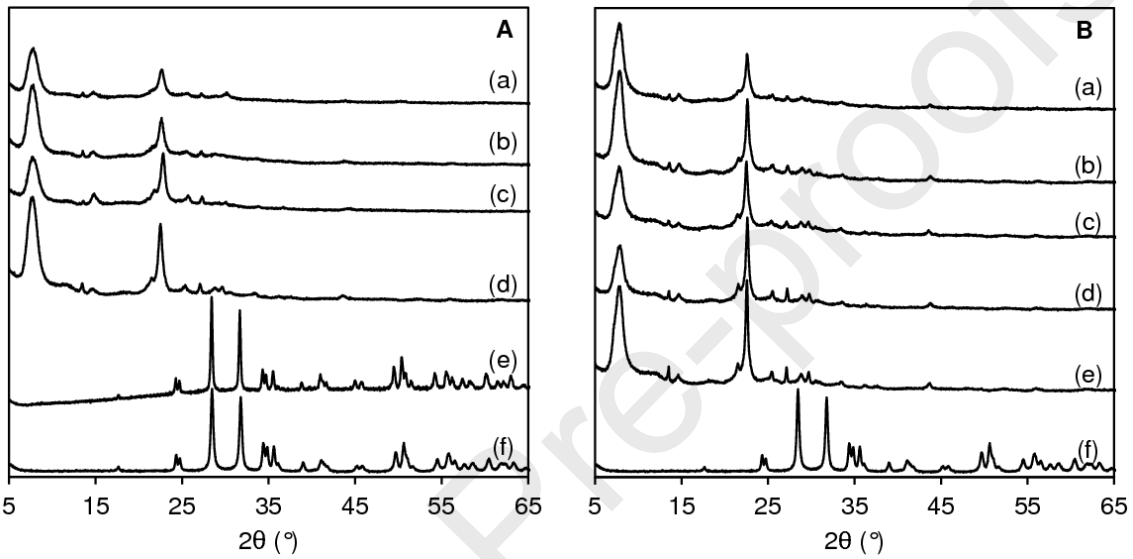

Fig. 1. PXRD patterns of the nanocrystalline (A) and microcrystalline (B) materials: (A) Zr-deAlBeta-n (a), Hf-deAlBeta-n (b), deAlBeta-n (c), H-Beta-n (d); (B) Hf-WdeSAlBeta-m (a), WdeSAlBeta-m (b), deSAlBeta-m (c), deAlBeta-m (d), H-Beta-m (e). The PXRD patterns of $Zr(acac)_4$ (A (e)) and $Hf(acac)_4$ ((f) in A and B) are shown for comparison.

The nitrogen sorption isotherms of the nanomaterials were of type I (Fig. 3(a)), characteristic of microporous materials according to the IUPAC classification [68]. The nanomaterials exhibited a slight H3 type hysteresis and increasing N_2 uptake as the relative pressure (p/p_0) approached unity, which may be due to some assemblages of slit-shaped pores [69]. The textural properties of the parent (H-Beta-n) and modified nanomaterials were roughly comparable; microporous volume (V_{micro}) in the range 0.1-0.15 $cm^3\ g^{-1}$ and external/mesoporous surface area (S_{EM}) in the range 247-299 $m^2\ g^{-1}$ (Table 2). The pore size distribution (PSD) curves of the nanomaterials were approximately coincident, in the range 2.5-10 nm (Fig. S4a).

The nitrogen sorption isotherms of the microcrystalline materials H-Beta-m, deAlBeta-m (Fig. 3b), Hf-Beta-m, deAl(HNO_3)Beta-m and Hf-deAl(HNO_3)Beta-m (Fig. S1B,E) were of type I and presented an increasing N_2 uptake at p/p_0 close to unity, which may be due to N_2 adsorption on the external surface (S_{EM} = 28-44 m^2 g^{-1}, Table 2). Desilicated deSAlBeta-m and the materials derived from it, exhibited type IV isotherms and a hysteresis (in the p/p_0 range of *ca.* 0.4-0.75) characteristic of mesoporous materials. The hysteresis loop is somewhat of type H2(a) where the desorption mechanism depends on the neck size, as well as on the connectivity to neighboring pores [70]. The S_{EM} increased from 44 m^2 g^{-1} for deAlBeta-m to 453 and 468 m^2 g^{-1} for deSAlBeta-m and WdeSAlBeta-m, respectively, which was accompanied by decreased microporosity (41-44 % of V_{micro} of deAlBeta-m was retained, Table 2); crystallinity seemed to decrease simultaneously.

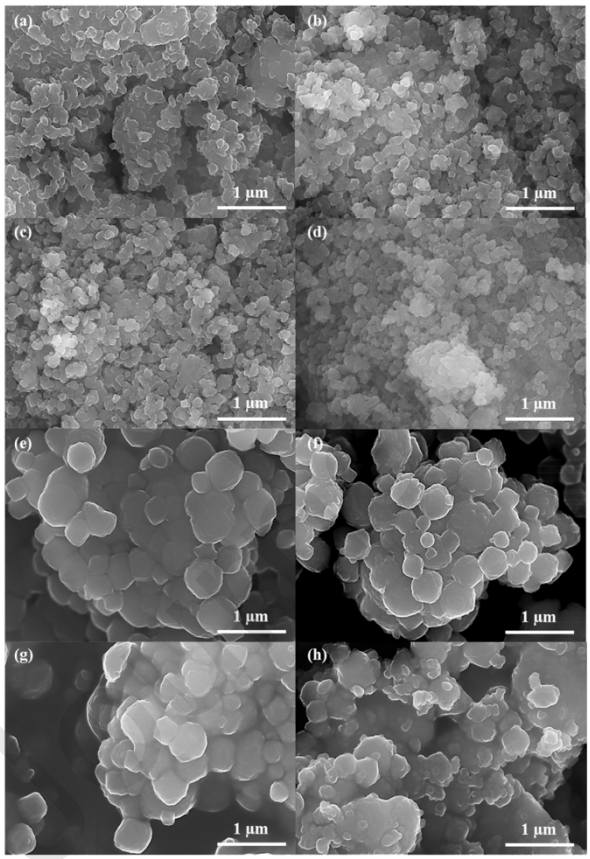

Fig. 2. SEM images of H-Beta-n (a), deAlBeta-n (b), Hf-deAlBeta-n (c), Zr-deAlBeta-n (d), H-Beta-m (e), deAlBeta-m (f), deSAlBeta-m (g), WdeSAlBeta-m (h), Hf-WdeSAlBeta-m (i).

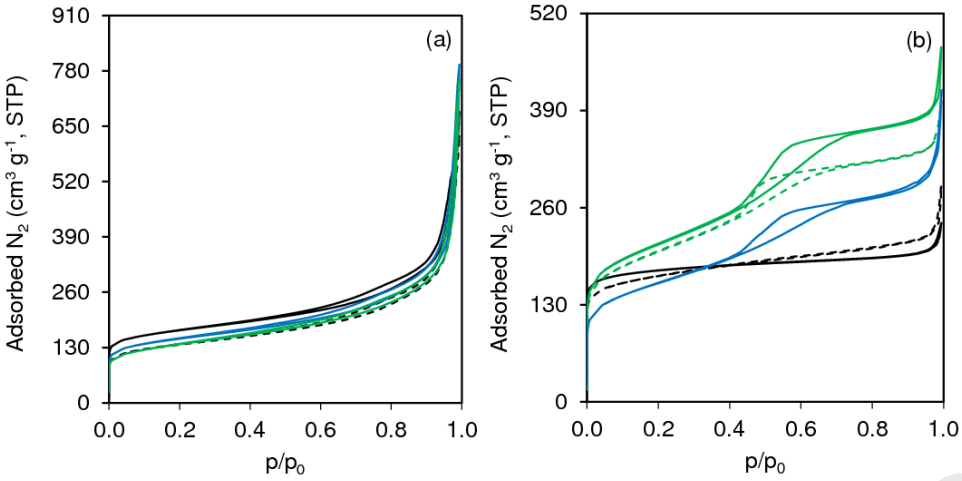

Fig. 3. Nitrogen adsorption isotherms of the (a) nanocrystalline BEA materials, namely, H-Beta-n (black solid line), deAlBeta-n (black dashed line), Hf-deAlBeta-n (blue solid line), Zr-deAlBeta-n (green solid line); and (b) microcrystalline BEA materials, namely, H-Beta-m (black), deAlBeta-m (black dashed line), deSAlBeta-m (green dashed line), WdeSAlBeta-m (green solid line), Hf-WdeSAlBeta-m (blue solid line).

Table 2. Textural properties of the prepared materials.

Sample	**S_{BET}** ($m^2\ g^{-1}$)	**S_{micro}** ($m^2\ g^{-1}$)	**S_{EM}** ($m^2\ g^{-1}$)	**V_p[a]** ($cm^3\ g^{-1}$)	**V_{micro}** ($cm^3\ g^{-1}$)	**V_M[a]** ($cm^3\ g^{-1}$)
H-Beta-n	625	378	247	1.06	0.15	0.91
deAlBeta-n	665	366	299	1.23	0.15	1.08
Hf-deAlBeta-n	541	290	251	1.23	0.12	1.11
Zr-deAlBeta-n	484	223	261	1.17	0.10	1.07
H-Beta-m	688	660	28	0.37	0.27	0.10
Hf-Beta-m	566	530	36	0.38	0.24	0.14
deAlBeta-m	627	583	44	0.45	0.27	0.18
deSAlBeta-m	723	270	453	0.62	0.11	0.51
WdeSAlBeta-m	759	291	468	0.73	0.12	0.61
Hf-WdeSAlBeta-m	564	173	397	0.64	0.08	0.56
deAl(HNO_3)Beta-m	598	560	39	0.44	0.25	0.19
Hf-deAl(HNO_3)Beta-m	589	559	31	0.36	0.24	0.12

[a] Comparison of these results between different samples may not be rigorous due to increasing N_2 uptake at p/p_0 close to unity [69].

Solely dealumination of H-Beta-m (giving deAl(HNO_3)Beta-m and Hf-deAl(HNO_3)Beta-m) was not effective for introducing mesoporosity. Instead, the desilication process effectively introduced mesoporosity in the particles giving Hf-WdeSAlBeta-m with S_{EM} of 397 m^2 g^{-1}. The PSD curves show mesopore sizes in the range 2.5-5 nm for Hf-WdeSAlBeta-m, which is somewhat narrower than that verified for Hf-deAlBeta-n (Fig. S4). Based on the above results, while the nanomaterials M-deAlBeta-n possess intercrystalline mesopores/voids, Hf-WdeSAlBeta-m possesses an intracrystalline hierarchical pore system, *i.e.* micro- and mesopores which make part of the crystal [71] (to denote this difference, in the present study, Hf-WdeSAlBeta-m is referred to as the hierarchical material).

A detailed discussion of DR UV-Vis (Fig. S5) and $^{29}Si\{^1H\}$ CP MAS NMR (Fig. S6) spectroscopies is given in the Supplementary Material, which, in summary, indicated differences in the surface chemistry between the M-containing zeotypes and the bulk transition metal oxides (Fig. S5; consistent with PXRD which did not reveal ZrO_2 and HfO_2 nanoparticles), and suggested the presence of silicon defect sites possessing silanol groups, and $Si(OSi)_3(O^-)$ or $Si(OSi)_2(OAl)(O^-)$ defects (Fig. S6).

The surface chemistry and structure of the M-sites of the zeotypes were studied by XPS spectroscopy. The XPS core level spectra of Hf-deAlBeta-n and Hf-WdeSiAlBeta-m are given in Fig. 4a and that of Zr-deAlBeta-n is given in Fig. 4b; the results for the bulk transition metal oxides were included for comparison. Bulk HfO_2 exhibited doublet signals corresponding to the electron energy levels Hf 4f7/2 and Hf 4f5/2 at *ca.* 18.5 and 16.8 eV, respectively (Fig. 4a), in agreement with literature data for hafnium oxide where each Hf atom may be coordinated with eight O atoms [72]. The Hf-zeotypes exhibited higher binding energies: *ca.* 21.0 and 20.0 eV corresponding to Hf 4f7/2 for Hf-deAlBeta-n and Hf-WdeSiAlBeta-m, respectively; and *ca.* 19.2 and 18.4 eV corresponding to Hf 4f5/2 for Hf-deAlBeta-n and Hf-WdeSiAlBeta-m, respectively. The higher binding energies for the Hf-zeotypes are assignable to framework (tetrahedral coordination) Hf sites, in parallel to that reported in the literature for Hf-USY [59], Hf-silicate [73] or Hf-SBA-15 [74].

Bulk ZrO_2 exhibited doublet signals at *ca.* 182.2 eV and 184.4 eV corresponding to Zr 3d5/2 and Zr 3d3/2, respectively (Fig. 4b). Higher binding energies were verified for ZrdeAlBeta-n (183.6 eV and 185.6 eV), which are attributable to framework (tetrahedral coordination) Zr sites, according to the literature for Zr-Beta type materials [55, 75, 76] and other silicates such as Zr-SBA-15 [77], Zr-MOR [78], Zr-KIT-5 [79], Zr-TUD-1 [80,

81], Zr-Al-SCM-1 [82]. The binding energy of Zr 3d5/2 (183.6 eV) for ZrdeAlBeta-n is close to that reported in the literature for $ZrSiO_4$ (183.3 eV), consistent with the formation of Si-O-M bonds during the SSI/calcination procedure [75]. Since silicon atoms possess a higher electronegativity than zirconium or hafnium, the presence of -O-Si groups in the coordination sphere of the M-sites (M-O-Si bonds) of the zeotypes may result in a greater withdrawal of electron density from the M-sites, making the latter more electron deficient than the M centers of the bulk transition metal oxides (are characterized by M-O-M bonds) [74, 76, 77, 83].

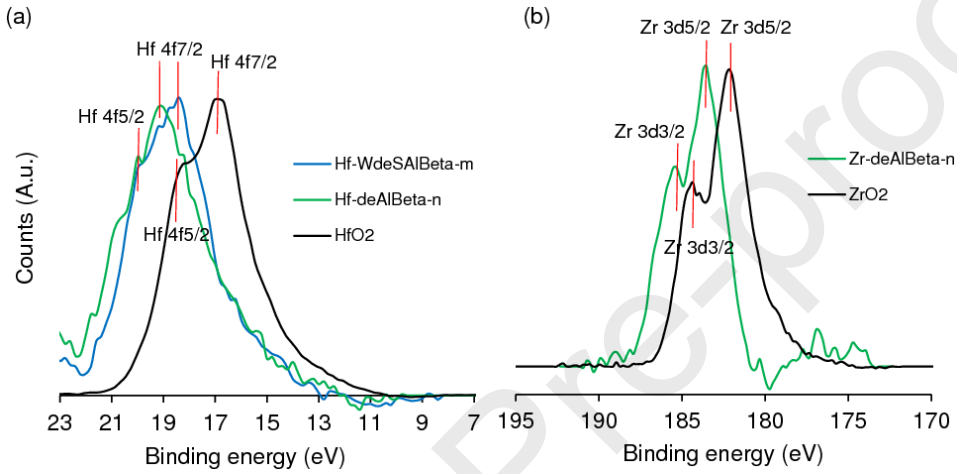

Fig. 4. Hf 4f (a) and Zr 3d (b) XPS core level spectra of the M-containing zeotypes and bulk HfO_2 (a) and ZrO_2 (b).

The XPS valence spectra of the zeotypes and bulk transition metal oxides were different due to the different surface chemical features of the two classes of materials (Fig. S7). The O1s core level profiles of the zeotypes (Fig. S8A) exhibited a significant shift of the binding energy to higher values (*ca.* 532.8 eV) in relation to the bulk metal oxides (*ca.* 530.1 eV for ZrO_2 and HfO_2, respectively), which is consistent with the different chemical environments of the M-sites of the zeotypes versus the bulk metal oxides. The signal at *ca.* 532.8 eV is due to Si-O bonds, according to the literature for various types of silicates [55, 59, 73, 77, 80, 84, 85]. The M-zeotypes and the respective dealuminated precursors deAlBeta-n and WdeSiAlBeta-m, exhibited similar Si 2p core level spectra, with a peak centred at *ca.* 103.8 eV (Fig. S8B), in agreement with literature data for BEA type materials (possess $\{SiO_4\}$ tetrahedra) [55]. Although the XPS analyses indicated the existence of tetrahedral M(IV) sites in the materials, one cannot exclude the possibility of, under the liquid phase catalytic reaction conditions, the M sites interacting with the

solvent molecules, leading to differences in their coordination environments and/or formation of defects with Lewis and/or Brønsted acidity [63, 86-88].

The acid properties of the materials were measured by FT-IR spectroscopy of adsorbed pyridine (at 150 °C) (Table 1). The amount of total acid sites of the parent zeolites H-Beta-n and H-Beta-m was 351 and 612 μmol g^{-1}, respectively, and they possessed a molar ratio L/B of 1.3. Although H-Beta-n and H-Beta-m possessed similar Si/Al ratio and S_{BET}, the former possessed a smaller amount of total acid sites than the latter, which may be partly associated with the fact that H-Beta-n consists of nano-sized particles and may possess a greater fraction of non-acidic defect sites. This hypothesis is supported by previous studies in which the H-Beta-n and H-Beta-m samples were analyzed by ^{27}Al MAS NMR spectroscopy; based on the areas of the peaks, the ratio [(pentacoordinated Al species)+(hexacoordinated Al species)]/(tetrahedral Al species) was equal to 0.28 and 0.40 for H-Beta-n and H-Beta-m, respectively [61, 89]. Although these results may not be rigorous due to possible presence of "NMR-invisible" Al species in zeolites [90], they suggest that H-Beta-n possessed a greater amount of hexacoordinated Al species (may be non-acidic). The amount of total acid sites of H-Beta-m decreased slightly upon SSI of Hf (giving Hf-Beta-m).

Dealumination of H-Beta-n led to a considerable reduction of the acidity, *i.e.*, deAlBeta-n possessed only few Brønsted (B) acid sites and no measurable Lewis (L) acidity. The SSI of M on deAlBeta-n furnished the material with B acidity and especially L acidity; specifically, M-deAlBeta-n possessed 42-73 μmol g^{-1} L acid sites and 4-20 μmol g^{-1} B acid sites. Zr-deAlbeta-n and deAlbeta-n possessed similar amounts of B acid sites, whereas Hf-deAlbeta-n possessed a greater amount of B acid sites than deAlbeta-n (20 and 7 μmol g^{-1}, respectively).

The dealuminated material WdeSAlBeta-m did not possess measurable acidity. The poor acidity of the precursors deAlBeta-n and WdeSAlBeta-m is consistent with their very high Si/Al ratios (510 and 697, respectively, Table 1); few Al-sites may be inaccessible to the base probe molecule and/or non-acidic defect sites. Somewhat in parallel to that for Hf-deAlBeta-n, the material Hf-WdeSAlBeta-m possessed enhanced L and B acidity compared to its precursor. The enhanced acidity of the Hf-containing catalysts is somewhat in agreement with the studies by Wang *et al.* [63] reporting that Hf(IV) sites in zeolite Beta may possess Lewis or Brønsted acidity. The affinities/reactivities of the Hf or Zr precursors with the zeolitic surface (*i.e.* the surface chemistry) may not be identical. For example, literature studies reported that hafnium may be more oxophilic

than zirconium inducing stronger Lewis [91] and/or Brønsted [92] acidity. On the other hand, it is known from the literature that Al sites with different coordination modes may interconvert by the influence of proximal water, different cations or organic molecules [90, 93, 94]. Future investigations (*e.g.*, computational studies) may elucidate the influence of hafnium on B acidity.

While the commercial zeolites H-Beta-n and H-Beta-m exhibited a band at 1455 cm^{-1} due to pyridine adsorbed on (classical zeolitic) L acid sites, which may be extra-framework and/or framework-associated aluminum species [93], the modified materials M-deAlbeta-n and Hf-WdeSAlBeta-m exhibited a lower frequency band (*ca.* 1448 cm^{-1}) assignable to the M-sites (Fig. S9). Literature studies for zeolites reported a lower frequency band due to weak L acid sites associated with alkaline or transition metal species [95]. The lower frequency band was not distinguishable in the spectrum of Hf-Beta-m due to the superimposed intense band at 1455 cm^{-1} associated with the (concentrated) Lewis acid Al-sites.

The above results suggest that the L acidity of M-deAlbeta-n and Hf-WdeSAlBeta-m is associated with M-sites. Accordingly, XPS spectroscopy indicated the presence of electron deficient M-sites in the zeotypes. To check the acid strength, the FT-IR spectra were recorded after evacuation at 350 °C (the amounts of L and B acid sites measured under these conditions are denoted L_{350} and B_{350}, respectively). The M-containing zeotypes and the respective dealuminated precursor materials deAlBeta-n and WdeSAlBeta-m did not possess strong B acidity (B_{350} = 0). The material Hf-WdeSAlBeta-m did not possess strong L acidity (L_{350} = 0). A comparison of the analogues M-deAlBeta-n indicated L_{350} = 0 for M = Zr, and a very small fraction of strong L acid sites was verified for M = Hf (L_{350}/L_{150} = 0.07). The acid properties of M-deAlbeta-n and Hf-WdeSAlBeta-m were also measured by NH_3-TPD, which gave similar profiles for the three samples (not shown), and a similar trend of the amount of total acid sites to that measured by FT-IR of adsorbed pyridine: Hf-WdeSAlBeta-m (215 μmol g^{-1}) > Hf-deAlbeta-n (173 μmol g^{-1}) > Zr-deAlbeta-n (118 μmol g^{-1}). The higher amounts of acid sites measured by NH_3-TPD compared to FT-IR of adsorbed pyridine may be partly due to the fact that NH_3 is a smaller base probe molecule than pyridine, and thus the former may access more (less accessible) acid sites.

3.2. Catalytic studies

3.2.1. Fur conversion to GVL

3.2.1.1.Catalysts M-deAlBeta-n with M = Hf versus Zr

Our group [55, 61, 62] and Winoto *et al.* [20, 21] reported the use of Zr- and Sn-Al-Beta zeolites as catalysts for the conversion of Fur via acid and reduction chemistry to bioproducts. One of the objectives of the present study was to produce GVL with improved yields, using Hf-containing Beta zeotypes as alternative stable catalysts. Hence, a comparison of the analogues M-deAlBeta-n with M = Zr or Hf (prepared under identical conditions) was firstly carried out. The two catalysts led to similar spectrum of bioproducts, namely 2BMF, AnL, LA, 2BL and GVL. However, the catalyst with M = Hf possessed a higher initial activity (9.1 and 5.3 mmol g_{cat}^{-1} h^{-1} for M = Hf and Zr, respectively) and turnover frequency (TOF; 32.5 mol mol_M^{-1} h^{-1} and 19.6 mol mol_M^{-1} h^{-1} for M = Hf and Zr, respectively), and led to greater total selectivity of bioproducts (up to 94 % total yield at 97 % Fur conversion for M = Hf, and up to 75 % total yield at 97 % conversion for M = Zr, using 2BuOH at 150 ºC). Moreover, the GVL yield was three times greater for M = Hf than for M = Zr, at 48 h/150 °C; 27 and 9 % yield, respectively (Fig. 5), and the carbon balance closed in 76 % and 66 %, respectively.

At a higher reaction temperature of 180 ºC, the differences in catalytic performances of the materials with M = Hf or Zr paralleled those verified at 150 ºC (Fig. 6). The GVL yield was more than 4 times greater for M = Hf than for M = Zr (42 and 9 %, respectively, at 180 ºC/24 h). Overall, the multifunctional catalyst Hf-deAlBeta-n performed superiorly to the analogue Zr-deAlBeta-n. These results correlate with the higher amounts of total acid (L+B) sites of Hf-deAlBeta-n in relation to Zr-deAlBeta-n (Table 1). Based on the mechanistic studies discussed below, and in agreement with literature studies, the M-sites may act as Lewis acid sites in the CTH steps of Fur to FA/AMF and of LA/ALs to GVL, and the B acidity may promote steps such as the furan-ring opening of FA/AMF to LA/ALs [20, 21, 46, 48, 49, 55, 62, 82, 96, 97]. Hence, adequate M-sites are required for triggering the reaction of Fur and forming GVL as target product of the integrated reaction process. The distinct catalytic roles of the M-sites of M-deAlBeta-n were further assessed by comparison with the precursor deAlBeta-n (without M) and the bulk transition metal oxides HfO_2 and ZrO_2. The bulk metal oxides led to similar or only slightly higher Fur conversion than without catalyst; 17 and 4 % conversion for HfO_2 and ZrO_2, respectively, and 2 % conversion without catalyst, at 24 h/150 °C. Hence, the zeotypes were remarkably superior catalysts, which correlated with the pronounced differences in structural and chemical properties of the two classes of materials (zeotypes versus bulk

metal oxides), as discussed in section 3.1. On the other hand, deAlBeta-n (without M) was very poorly active (9 % conversion at 24 h/150 °C) because it did not possess measurable L acidity (Table 1) and therefore failed to trigger the reaction of Fur.

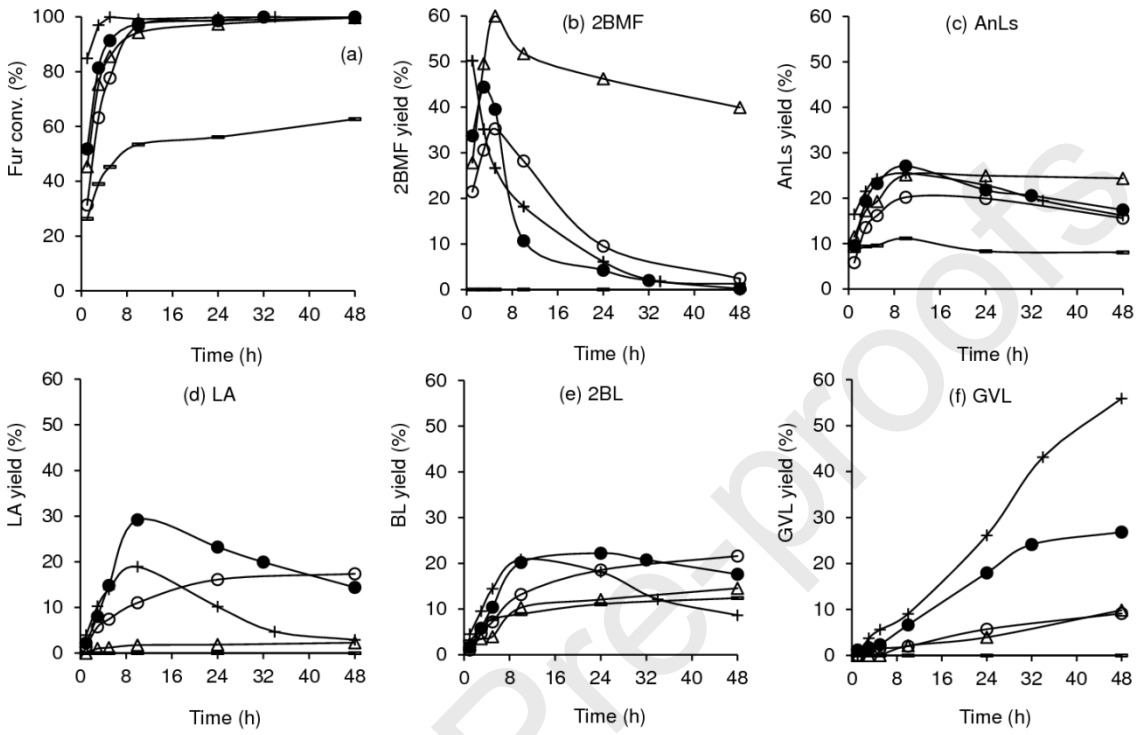

Fig. 5. Conversion of Fur (a) to the bioproducts 2BMF (b), AnLs (c), LA (d), 2BL (e) and GVL (f) (FA yields were less than 2 %), in the presence of Hf-deAlBeta-n (•), Zr-deAlBeta-n (o), Hf-WdeSAlBeta-m (+), Hf-Beta-m (-) or Hf-deAl(HNO_3)Beta-m (Δ), using 2BuOH at 150 °C.

3.2.1.2. Reaction mechanism and kinetic modelling

Mechanistic considerations may be drawn from a careful analysis of the kinetic curves of the reaction of Fur, in the presence of Hf-deAlBeta-n, at 150 ºC (Fig. S10A). The distribution of bioproducts changed as conversion increased, suggesting that a complex reaction mechanism was involved. The kinetic curves of the formation of 2BMF, AnL, LA and 2BL presented a maximum, whereas the curve of GVL presented an induction period and afterwards it increased with time. These profiles suggest that 2BMF, AnL, LA and 2BL were intermediates of the conversion of Fur to GVL. The maximum of the kinetic curve of 2BMF formation (44 % yield at 81 % conversion) was reached before the maximum concentrations of AnL, 2BL and LA were reached, suggesting that 2BMF was an earlier intermediate of the overall reaction. These results are consistent with the

literature in that AMFs may be converted to alkyl levulinates (ALs) [20, 45, 46, 48, 50, 53-56, 60, 62, 82, 97-102], LA [45, 46, 48, 54, 60, 82, 97, 99, 100] or AnLs [20, 21, 46, 53, 55, 62, 97, 98, 102].

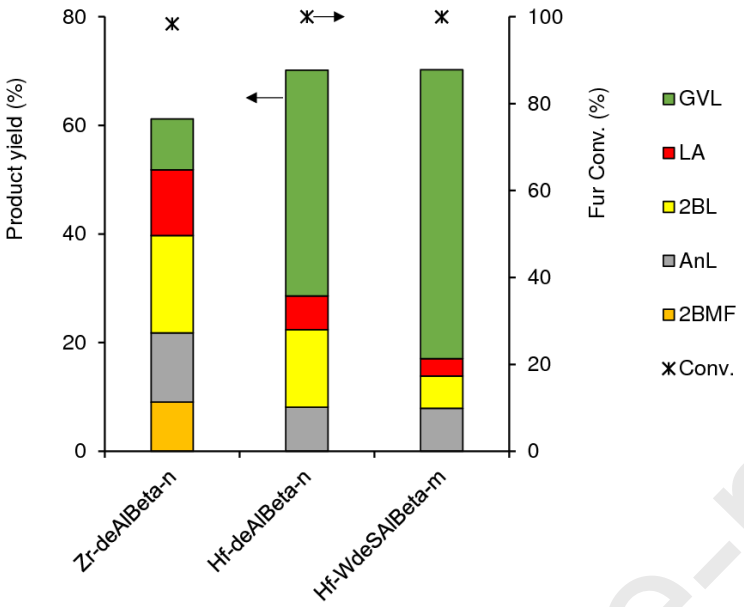

Fig. 6. Conversion of Fur (*) to bioproducts (bars), in the presence of M-deAlBeta-n or Hf-WdeSAlBeta-m, using 2BuOH at 180 ºC, 24 h.

Based on the above results and literature studies for the reaction of Fur-to-GVL [21, 55, 62], a plausible overall reaction mechanism is presented in Scheme 2. This mechanism is also supported by the results discussed below in sections 3.2.2 and 3.2.3 for different substrates (AnL and LA). Scheme 2 presents some routes which are in agreement with previous studies by our group and Winoto *et al*. (the latter did not report kinetic modelling studies) for modified BEA catalysts, where the intermediate bioproducts included AnL [21, 55, 62]. The mechanism in Scheme 2 contemplates the formation of by-products because the carbon balance did not close (discussed in section 3.2.1.1). The complexity of the mechanism partly resides in the fact that water is coproduct of some elementary steps (*e.g.*, etherification of FA to 2BMF) which may participate in parallel routes such as the conversion of FA to LA (without the intermediate formation of AMFs). LA may be formed from FA with or without the intermediate formation of AnL, in agreement with different studies reported in the literature [46, 55, 62, 103]. On the other hand, LA/ALs may be formed from AMFs with or without the intermediate formation of AnL [20, 45, 50, 51, 54-56, 60, 62, 82, 97, 98, 100, 101]. ALs may also be formed via esterification of

LA [20, 21, 49, 55, 62, 96]. Finally, the desired product GVL may be formed from LA [104, 105] or ALs [106, 107].

Based on Scheme 2, a kinetic model was developed. The experimental and calculated kinetic curves of the reaction of Fur are shown in Fig. S10A, and the calculated rate constants (k_j) are indicated in Table S1. The kinetic model fitted reasonably well the experimental data (F_{obj} = 0.0032), and thus the proposed mechanism seems plausible and reasonable. It fitted better the experimental results than, for example, the model/mechanism reported previously by our group [55, 62]. The fastest step of the overall process was the conversion of FA to 2BMF (k_2), which is consistent with the fact that FA was present in very small amounts throughout the reaction, *i.e.* it is a considerably reactive intermediate (in agreement with the literature [55, 62]) and is converted as it is formed. The ring-opening of 2BMF to 2BL (k_6) or LA (k_7) was faster than that of 2BMF to AnLs (k_5). On the other hand, the conversion of 2BMF to 2BL (k_6) was faster than the esterification of LA to 2BL (k_9). Finally, GVL was formed from 2BL (k_{11}) and especially LA ($k_{10} > k_{11}$).

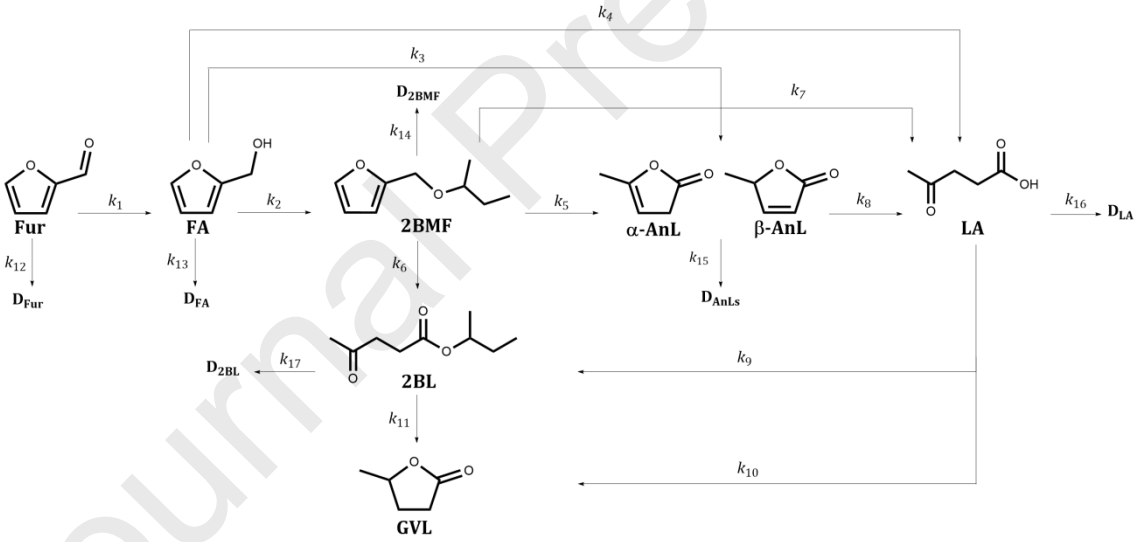

Scheme 2. Overall reaction mechanism proposed for the reaction of Fur to bioproducts, in the presence of M-deAlBeta-n or Hf-WdeSAlBeta-m, in alcohol medium.

3.2.1.3. Aliphatic alcohol effect

2-Butanol and 2-propanol (2PrOH) are two of the most effective and studied H-donor alcohols for conversion processes involving CTH chemistry, related to carbohydrate biomass derived compounds [42, 47, 50, 51, 59, 108, 109], and the two alcohols may be produced from vegetable biomass [110-112]. Hence, the performance of Hf-deAlBeta-n was further investigated using these H-donors, at 150 ºC (Fig. 7). For the two Fur/alcohol

systems, the product spectrum was similar, suggesting that a similar reaction mechanism is involved. The bioproducts were the corresponding 2-(alkoxymethy)furans (AMFs), alkyl levulinates (ALs), AnLs, LA and GVL. The initial activity and TOF of Hf-deAlBeta-n were higher for Fur/2BuOH (9.1 mmol g_{cat}^{-1} h^{-1} and 32.5 mol mol_{Hf}^{-1} h^{-1}) than for Fur/2PrOH (6.3 mmol g_{cat}^{-1} h^{-1} and 22.5 mol mol_{Hf}^{-1} h^{-1}). This tendency parallels that reported in the literature for the catalysts Sn-deAlbeta [62], ZrAl-Beta/TUD-1 [61] and Sn,Al-Beta [20] tested for the same catalytic reaction. On the other hand, the system Fur/2BuOH led to a higher GVL yield at 24 h than Fur/2PrOH (18 and 7 % yield, respectively, at 100 % conversion), and the yield of total bioproducts was slightly higher for the former. Hence, 2BuOH seems to be a more favourable H-donor agent.

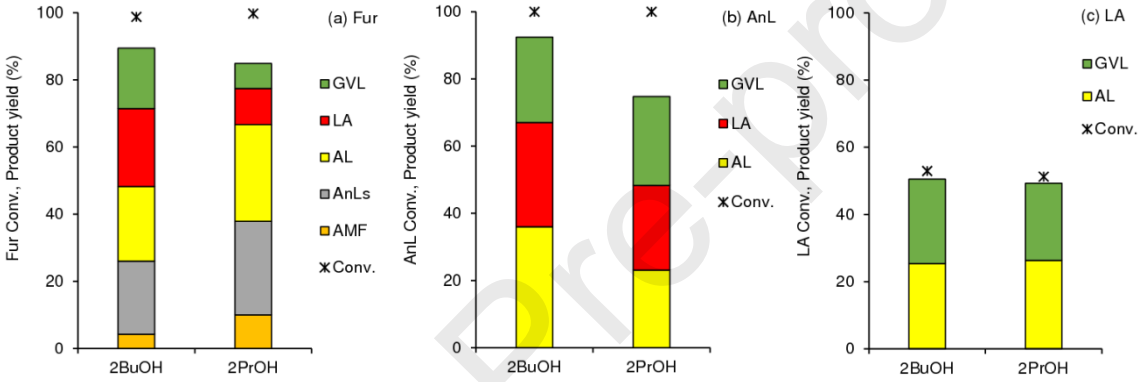

Fig. 7. Conversion of Fur (a), AnL (b) and LA (c) to the corresponding bioproducts (bars), in the presence of Hf-deAlBeta-n, using 2BuOH or 2PrOH at 150 °C (24 h).

3.2.1.4. Different versions of Hf-containing catalysts

Since catalytic performances may depend not only on the acidity, but also on the textural and morphological properties of the materials, the introduction of hierarchy in the zeolite crystals is worth pursuing as a means to improve GVL production. Hence, we prepared the first hafnium-containing BEA zeotype possessing an intracrystalline hierarchical pore system, namely Hf-WdeSAlBeta-m, and tested this material for GVL production (Fig. 5). The initial activity and TOF for Hf-WdeSAl-Beta-m (14.9 mmol g_{cat}^{-1} h^{-1} and 51.7 mol mol_{Hf}^{-1} h^{-1}) were higher than for Hf-deAlBeta-n (9.1 mmol g_{cat}^{-1} h^{-1} and 32.5 mol mol_{Hf}^{-1} h^{-1}), and higher GVL yields were reached for the former. Specifically, 56 and 27 % GVL yield was reached at 48 h/150 °C for Hf-WdeSAl-Beta-m and Hf-deAlBeta-n, respectively (Fig. 5f), and the carbon balance closed in 85 % and 76 %, respectively. The higher activity of Hf-WdeSAlBeta-m correlates with its higher amount of total (L+B) acid

sites (Table 1). According to the literature for Fur conversion to GVL over zeolites, the L/B molar ratio may be optimised to favour GVL formation [48, 82]. The L/B ratio of Hf-WdeSAl-Beta-m (6.3) is intermediate between those of Hf-deAlBeta-n (3.7) and Zr-deAlBeta-n (10.5). On the other hand, the superior performance of Hf-WdeSAl-Beta-m may be due to its considerably higher external/mesoporous specific surface area (S_{EM} = 397 compared to 251 m^2 g^{-1} for Hf-deAlBeta-n, Table 2). Enhanced S_{EM} may facilitate the accessibility of the reactants to the active sites and enhance the adsorption of the reactants and intermediates on the catalyst surface close to the active sites, favouring the consecutive reactions that lead to GVL.

The product spectrum was similar for Hf-WdeSAl-Beta-m and Hf-deAlBeta-n, suggesting that a similar reaction mechanism is involved. Hence, the kinetic model fitted reasonably well the experimental data for Hf-WdeSAl-Beta-m (Fig. S10B, Table S1). The model predicted that k_1 (Fur conversion, Table S1) was greater for Hf-WdeSAlBeta-m which possessed a higher amount of total acid sites than Hf-deAlBeta-n (Table 1). In parallel to that verified for Hf-deAlBeta-n, for Hf-WdeSAl-Beta-m the fastest step was the conversion of FA to 2BMF (k_2), and the conversion of 2BMF to 2BL (k_6) or LA (k_7) was faster than 2BMF to AnLs (k_5). The much faster 2BL to GVL over Hf-WdeSAlBeta-m than Hf-deAlBeta-n (two orders of magnitude difference in k_{11}, Table S1), contributed to enhanced GVL formation in the former case.

Higher GVL yields were reached at 180 ºC in the presence of Hf-WdeSAl-Beta-m (56 % and 73 % at 150 ºC and 180 ºC respectively, 48 h), and the kinetic profiles presented comparable tendencies to those seen for the reaction temperature of 150 ºC, suggesting that the overall mechanism is similar (Fig. 5 and Fig. S11). At 180 ºC, the performance of the hierarchical catalyst Hf-WdeSAlBeta-m was again superior to that of Hf-deAlBeta-n.

From a practical point of view, it is desirable to avoid the etherification of the aliphatic alcohol solvent. For Hf-deAlBeta-n and Hf-WdeSAlBeta-m, 2BuOH was converted to 2-*sec*-butoxybutane (BB) in less than 0.5 % yield (based on the initial molar amount of solvent) at 150 ºC/24 h, and less than 1% yield at 180 ºC/24 h. The amount of BB formed per amount of desired product (GVL) gives an idea of the possible level of product contamination caused by solvent degradation. At 150 ºC, the molar ratio BB:GVL was similar for the two catalysts (0.39-0.43), whereas at 180 ºC, the molar ratio was higher for Hf-deAlBeta-n than Hf-WdeSAlBeta-m (*ca.* 0.57 and 0.26, respectively).

For comparison, a catalytic test was carried out using a mechanical mixture of WdeSAlBeta-m plus HfO_2, which gave 3 % Fur conversion at 24 h/150 °C and no GVL was formed. These results assess the importance of incorporating hafnium in the dealuminated/desilicated hierarchical zeotype structure, for the catalytic conversion of Fur to GVL. To further support this hypothesis, the SSI of hafnium was carried out (similarly to that for Hf-WdeSAlBeta-m) on (i) commercial H-Beta-m giving Hf-Beta-m, (ii) ordered mesoporous silica, giving Hf-MCM-41 and (iii) dealuminated, non-desilicated Hf-deAl(HNO_3)Beta-m.

Hf-Beta-m led to relatively slow Fur reaction at 150 °C, and did not give GVL (Fig. 5). The initial activities of Hf-Beta-m and Hf-WdeSAl-Beta-m were 4.4 and 14.9 mmol g_{cat}^{-1} h^{-1}, respectively, and the TOFs were 15.6 and 51.7 mol mol_{Hf}^{-1} h^{-1}, respectively. Hf-Beta-m led to 63 % conversion at 48 h, whereas Hf-WdeSAl-Beta-m led to 100 % conversion within 24 h. Moreover, Hf-Beta-m led to AnL and 2BL (8 and 12 % yield at 48 h), but not 2BMF, LA and GVL, and the reaction was poorly selective (33 % total selectivity at 63 % Fur conversion for Hf-Beta-m, compared to more than 80 % total selectivity at 100 % conversion for Hf-WdeSAl-Beta-m). These results may be partly due to the fact that Hf-Beta-m possessed much more acid sites than Hf-WdeSAlBeta-m, albeit much lower S_{EM} (Table 1 and Table 2).

Somewhat in parallel to Hf-Beta-m, Hf-MCM-41 led to slower Fur reaction (initial activity = 4.5 mmol g_{cat}^{-1} h^{-1}) than Hf-WdeSAl-Beta-m, low total selectivity to bioproducts (60 % at 96 % conversion, at 150 °C/24 h), and did not give GVL (instead, 2BMF, AnL, LA and 2BL were formed in 13, 18, 4 and 22 % yield, respectively); the mechanical mixture of MCM-41 plus HfO_2 led to sluggish Fur reaction (7 % conversion at 24 h). These results may be due to interplay of different factors: *e.g.*, Hf-MCM-41 possessed higher mesoporous specific surface area (623 m^2 g^{-1}), inferior acidity (27 μmol g^{-1} L acid sites, no B acidity, Supplementary Material) and non-crystalline pore walls (*i.e.*, lacks precise atomic positioning), whereas Hf-WdeSAl-Beta-m has a crystalline framework (S_{EM} = 397 m^2 g^{-1}, 110 μmol g^{-1} acid sites) [113, 114].

The dealuminated, non-desilicated zeotype Hf-deAl(HNO_3)Beta-m was less active (initial activity = 7.7 mmol g_{cat}^{-1} h^{-1}) than Hf-WdeSAl-Beta-m and led mainly to 2BMF (46 % yield at 150 °C/24 h, Fig. 5b), presenting poor effectiveness for carrying out consecutive reactions which lead to GVL (4 % yield at 24 h). These results correlate with the fact that Hf-deAl(HNO_3)Beta-m possessed only 8 % of the mesoporous specific

surface area of Hf-WdeSAl-Beta-m (Table 2), and somewhat lower acidity (L+B = 70 μmol g^{-1} (L/B= 6), Table 1). The above results support the importance of incorporating hafnium in the dealuminated/desilicated hierarchical zeotype structure in order to confer favourable activity for GVL synthesis. With the development of the mesoporosity, some surface regions may be ordered at the atomic scale (BEA topology) and others may be disordered (amorphous). The exact location of the Hf sites is not clear, but it is possible that the accessible Hf sites on the crystalline and/or amorphous surface regions may possess somewhat different electronic properties, which may influence the intrinsic activity.

3.2.1.5. Hf-catalysts compared to other catalysts

To the best of our knowledge there are only two studies which used hafnium-based catalysts (MOFs) for the one-pot conversion of Fur to GVL. Specifically, Hf-MOF-808 had to be mechanically combined with another catalyst, Al-Beta (in 2BuOH) [56], and sulfated DUT-67(Hf)-0.06 was prepared via a post-synthesis treatment with H_2SO_4 (the same treatment had to be performed prior to catalyst reuse to preserve the catalytic activity) [60]. Table S2 shows the results for Hf-WdeSAlBeta-m and literature data for different heterogeneous catalysts tested for Fur conversion to GVL, using secondary alcohol solvents. The different studies employed different reaction conditions (temperature, time, catalyst:Fur mass ratio, initial concentration of Fur and type of alcohol solvent), which influences the catalytic reaction, making it difficult to establish clear comparisons. On the other hand, the catalyst´s composition and stability are important factors that may also influence the catalyst productivity. Hence, Table S2 is not intended to rank the catalysts, but it shows that different types of non-noble metal catalysts were studied: fully inorganic (*e.g.* zeolites, mesoporous silicates) and organic-inorganic hybrids (*e.g.* MOFs), and sometimes mechanical mixtures of two catalysts were used [20, 21, 45, 46, 48-54, 56, 60, 82, 96-102, 115-118]. GVL yields ranged from 11 % at 24 h/150 ºC (using HPMo(20)/Zr-MCM-41 in a mass ratio catalyst:Fur = 8.33, entry 25 [117]) to 87 % at 24 h/180 ºC (using DUT-67(Hf)-0.06 in a mass ratio catalyst:Fur = 2.5, entry 22 [60]), 88 % at 10 h/170 ºC (20%Zr-5%T-Beta; mass ratio catalyst:Fur = 0.765, entry 10 [51]) and 90 % at 24 h/120 ºC (using meso-ZrAl-Beta; mass ratio catalyst:Fur = 2.5, entry 8 [48]). The catalyst Hf-WdeSAlBeta-m (4.8 wt% Hf) led to 73 % GVL yield at 48 h/180 ºC (mass ratio catalyst:Fur = 0.59) and was stable (discussed below). For comparisons in a different perspective, separate catalytic tests were carried out for Hf-WdeSAlBeta-m

under selected conditions based on Table S2. Under similar conditions to those of entry 22 (catalyst:Fur = 2.5, 2PrOH, 24 h, 180 ºC), the Fur/2BuOH reaction in the presence of Hf-WdeSAlBeta-m gave 86 % GVL yield at 100 % conversion, which is similar to that reported for the sulfated DUT-67(Hf)-0.06 catalyst (87 % GVL yield) [60]. Decreasing the reaction temperature to 120 ºC (conditions of entry 8), the GVL yield decreased considerably to 10 % for Hf-WdeSAlBeta-m, which is much lower than that reported for meso-ZrAl-Beta prepared via acid and alkaline treatments and SSI with zirconocene dichloride and calcination (90 % GVL yield at 24 h/120 ºC) [48]; the chloride content in the prepared catalyst and its possible influence on the catalytic reaction were not reported. Under similar conditions to those of entry 10 (catalyst:Fur = 0.765, 2PrOH, 10 h, 170 ºC), the Fur/2BuOH reaction in the presence of Hf-WdeSAlBeta-m (Si/Hf = 44) gave 51 %, which is less than that reported for zeolite Beta with relatively high loadings of ZrO_2 plus 12-tungstophosphoric acid (25 wt% in total; 88 % GVL yield [51]). Reasonably, it is difficult to fully reproduce catalytic results of different groups, and thus these comparisons may not be a representative ranking. Additionally, the economic and scaling up feasibility of the different catalyst synthesis protocols may have practical impacts and should be considered. Importantly, changing the transition metal from, for example, typically used Sn or Zr, to Hf in the development of heterogeneous catalysts for Fur to GVL, may enhance the productivity.

3.2.2. Substrate scope - AnL reaction

The M-deAlBeta-n and Hf-WdeSAlBeta-m materials were further studied for the conversion of AnL to GVL, in alcohol medium at 150 °C or 180 °C. The main products were LA, ALs and GVL (Fig. 8 and Fig. S12). The reaction AnL/2BuOH in the presence of Hf-deAlBeta-n gave 25 % GVL yield at 24 h, 150 °C, which was greater than that for the analogue Zr-deAlBeta-n (14 % yield, Fig. 8). Increasing the reaction temperature from 150 °C to 180 °C led to higher GVL yields, especially for M = Hf. Specifically, for M = Hf, GVL yield after 24 h rose to 60 %, whereas for M = Zr the GVL yield increased to 27 % at the higher temperature (Fig. 8). The type of alcohol did not influence significantly the GVL yield, albeit the total yield of bioproducts was higher for AnL/2BuOH than AnL/2PrOH (95 and 80 % total yield, respectively, at 100 % conversion, 150 °C/24 h, in the presence of Hf-deAlBeta-n; Fig. 7b). Hence, the system AnL/2BuOH was more selective. Higher GVL yields were reached with AnL than with Fur as substrate (Fig. 5),

which may be partly because the route starting from AnL is shorter than that of Fur to GVL (Scheme 2).

The catalyst Hf-WdeSAlBeta-m possessing interconnected hierarchical pore system performed superiorly to Hf-deAlBeta-n in the reaction of AnL (Fig. 8 and Fig. S12), in parallel to that verified with Fur as substrate (Fig. 5); Hf-WdeSAlBeta-m led to 32 %/91 % GVL yield, at 150 °C/180 °C, 24 h (Fig. 8).

Table 3 lists the catalytic results for Hf-WdeSAlBeta-m and other heterogeneous catalysts reported in the literature for the reaction of AnL using a secondary alcohol as H-donor [20, 55, 62, 119]. To the best of our knowledge, only three studies were reported, two of them by our group [55, 62]. Beta zeotypes possessing 10 wt% of Sn or Zr led to less than 4% GVL at 120 °C (entries 3, 4) [55, 62]. A SnAl-Beta catalyst prepared via dealumination and SSI using dimethyltin dichloride, led to 33 % GVL yield at 160 °C/6 h (entry 5) [20]. Catalyst Hf-WdeSAlBeta-m led to a similar GVL yield of 32 % at 150 °C/24 h, even though it was used in a lower catalyst:substrate mass ratio of 0.61 and was prepared using half the amount of transition metal precursor (per gram of zeolite) than that used in ref. [20]. The mesoporous silicate Zr-TUD-1 led to less than 1 % GVL yield at 120 °C/7 h (entry 7) [55]. Zeolite H-Beta catalyst (without transition metal) did not give any GVL in the reaction AnL/2PrOH at 110 °C/1.5 h (entry 6) [119].

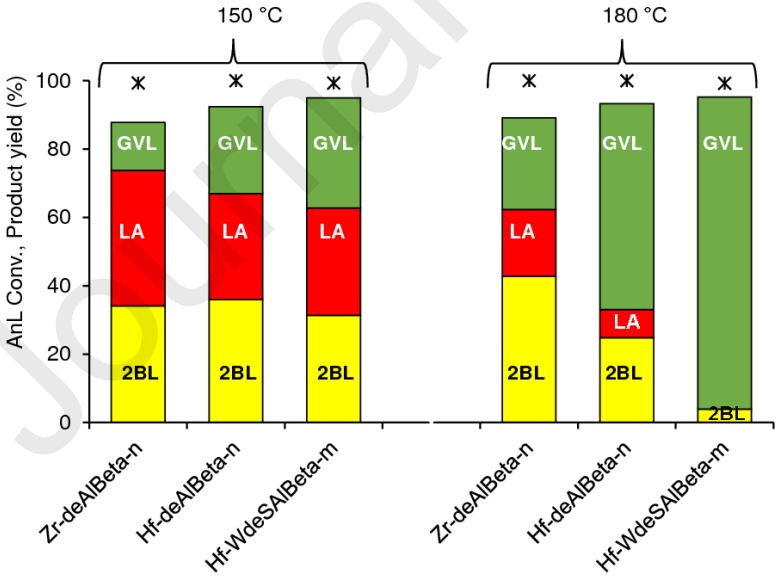

Fig. 8. Conversion (*) of AnL, in the presence of M-deAlBeta-n or Hf-WdeSAlBeta-m, to the bioproducts 2BL, LA and GVL, using 2BuOH at 150 °C or 180 °C (24 h).

Table 3. Catalytic results for Hf-WdeSAlBeta-m and other catalysts reported in the literature for the reaction of AnL to GVL, using a secondary alcohol as H-donor (without external supply of H_2).

Entry	Catalyst	Solvent	T (ºC)	t (h)	$[AnL]_0$ (M)	Cat:AnL (m/m)	Conv. (%)	Yield GVL (%)	Ref
1	Hf-WdeSiAlBeta-m	2BuOH	150	24	0.45	0.61	100	32	Here
2	Hf-WdeSiAlBeta-m	2BuOH	180	24	0.45	0.61	100	91	Here
3	$(Zr)_{SSIE}$-Beta-n(10wt%Zr)	2BuOH	120	7	0.45	0.61	99	3	[55]
4	$(Sn)_{SSIE}$-Beta(10wt%Sn)	2BuOH	120	7	0.45	0.61	99	2	[62]
5	SnAl-Beta-14	2PrOH	160	6	0.11	0.74	86	33	[20]
6	H-Beta	2PrOH	110	1.5	0.29	0.40	99	0	[119]
7	Zr-TUD-1	2BuOH	120	7	0.45	0.61	98	<1	[55]

3.2.3. Substrate scope - LA reaction

The conversion of LA to GVL, in the presence of Hf-deAlBeta-n or Hf-WdeSAlBeta-m, in alcohol media at 150 °C or 180 °C, gave mainly the corresponding ALs and GVL. Based on conversion at 24 h, LA was less reactive than the substrates Fur or AnL (Fig. 9 versus Fig. 6 and Fig. 8).

The type of alcohol (2BuOH or 2PrOH) did not influence significantly the GVL yields; 23-25 %, at 24 h/150 °C, in the presence of Hf-deAlBeta-n (Fig. 7c). Increasing the temperature from 150 °C to 180 °C led to a considerable increase of GVL yield (Fig. 9), and Hf-deAlBeta-n performed superiorly to its analogue with M = Zr; 25 %/80 % GVL yield at 150 °C/180 °C for M = Hf, compared to 13 %/21 % GVL yield for M = Zr. Overall, higher GVL yields were reached for the catalyst possessing M = Hf, starting from Fur, AnL or LA. For the reaction LA/2BuOH/180 °C, the GVL yield increased from 80 to 95 % between 24 and 48 h, whereas 2BL yield decreased from 12 to 2 %. The amount of converted LA (5 %) plus the amount of 2BL consumed (10 %) between 24 and 48 h, equals the increase in GVL yield of 15 % in the same period of time. These are consistent with the proposed mechanism (Scheme 2) in that GVL may be formed from LA or 2BL.

The catalyst Hf-WdeSAlBeta-m showed superior performance at the higher reaction temperature of 180 °C, leading to a GVL yield of 99 % after 24 h reaction (Fig. 9).

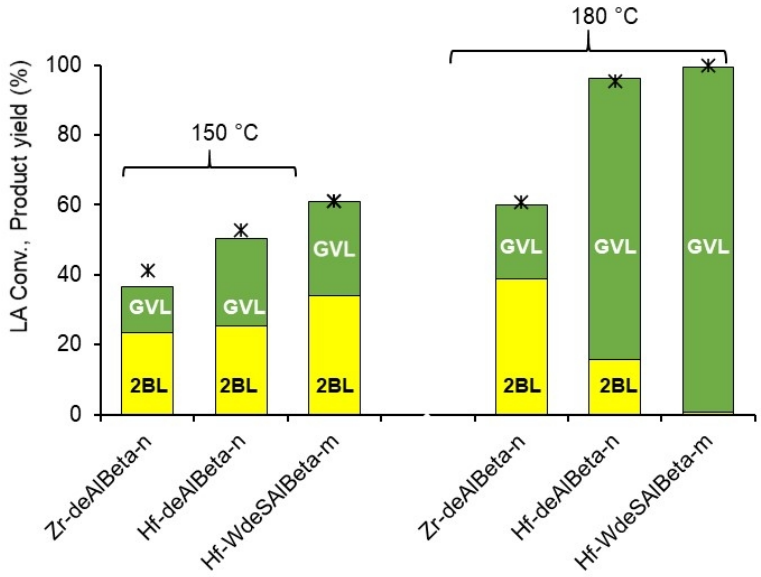

Fig. 9. Conversion (*) of LA, in the presence of M-deAlBeta-n or Hf-WdeSAlBeta-m, to the bioproducts 2BL and GVL, using 2BuOH at 150 °C or 180 °C (24 h).

The reaction of LA to GVL was extensively studied in the literature, using a large variety of catalysts, and secondary alcohols [120] or formic acid [35] as *in situ* hydrogen sources, or using externally supplied molecular hydrogen [121]. The types of catalysts tested for LA/(2PrOH or 2BuOH) to GVL ranged from zeolites/zeotypes, silicates and (mixed) metal oxides [42, 122-125] to noble metal/carbon catalysts [109, 126-129], hafnium-graphite oxide [130], organic-inorganic hybrids and MOFs [107, 131-134]. Table S3 lists the catalytic results for Hf-WdeSAlBeta-m (27 %/99 % GVL yield at 150 ºC/180 ºC, 24 h) and other zeolitic catalysts reported in the literature for the reaction of LA using a secondary alcohol H-donor [20, 21, 49, 54, 55, 59, 61, 62, 100, 135, 136]. Very high yields (> 90 %) were reported for some zeolites, namely Hf-USY which led to 95 % GVL yield at 10 h/150 °C (catalyst:LA mass ratio = 0.86, 2PrOH; entry 14) [59] and Zr-Beta (synthesised using HF, 40 days) which led to 97 % GVL yield at 11 h/120 °C (catalyst:LA mass ratio = 0.64, 2BuOH; entry 7) [54].

3.2.4. Catalyst stability

The catalytic stability of Hf-deAlbeta-n and Hf-WdeSAlBeta-m was studied via catalyst reuse, contact tests and characterisation of the solids recovered from the reaction of Fur at 180 °C/24 h, in 2BuOH. The thermal analyses indicated that the used catalysts Hf-deAlbeta-n and Hf-WdeSAlBeta-m presented a weight loss of 29 and 17 %, respectively

(200-750 ºC, Fig. S13a-b). The used catalysts exhibited two exothermic peaks centred at *ca.* 350 and 470 ºC, which did not appear for the fresh catalysts (Fig. S13c-d) and may be due to the decomposition of organic matter. Elemental analysis indicated a carbon content of 20 and 9 wt% for the used catalysts Hf-deAlbeta-n and Hf-WdeSAlBeta-m, respectively. Hence, coke formation was evidently more important for the nanocrystalline material than for the hierarchical catalyst Hf-WdeSAlBeta-m. The contact tests (details in the experimental section) indicated that Fur conversion (in homogeneous phase) at 24 h was 17 and 6 % for Hf-deAlbeta-n and Hf-WdeSAlBeta-m, respectively, whereas for a normal catalytic test, conversion at 1 h was 89 % for Hf-deAlbeta-n and 98 % for Hf-WdeSAlBeta-m. Hence, the two materials were essentially heterogeneous catalysts. The slightly higher value of conversion (17 %) for the contact test of Hf-deAlbeta-n may be due to some nanoparticles which were not completely separated (*ca*. 220 nm pore size membrane was used).

Hf-deAlbeta-n and Hf-WdeSAlBeta-m performed relatively steadily in four consecutive batch runs (Fig. 10). The crystalline structure (Fig. S14), morphological features (Fig. S15), Si/Al and Si/Hf molar ratios (Table S4) and elemental distributions (Fig. S16) were similar for the fresh and used catalysts. The total amount of acid sites varied slightly by a factor of *ca.* 1.1 and the L/B ratio remained similar (Table S5) for the fresh/used catalysts. The textural properties of the fresh/used catalysts Hf-deAlbeta-n and Hf-WdeSAlBeta-m were preserved (Table S6). Additional catalyst stability tests were carried out for Hf-WdeSAlBeta-m with LA as substrate (180 ºC) to check the stability at lower conversions (Fig. S17). LA conversion and GVL yield increased especially in the first three consecutive 5-hour batch runs and afterwards tended to similar values (79 % GVL yield at 97 % LA conversion, 5 h, in run 5). There seemed to exist some influence of the type of substrate, since this effect was not verified for the recycling runs with Fur. However, the crystalline structure, textural and acid properties of the used catalyst were essentially preserved, in parallel to that verified with Fur as substrate (Figure S14, Tables S5 and S6). Possibly, in the presence of the organic acid (LA) some surface alterations may occur *in situ*, which were not evidenced in the (solid-state) characterization studies of the used solids. Future *in situ* characterization and/or computational studies may possibly elucidate these effects.

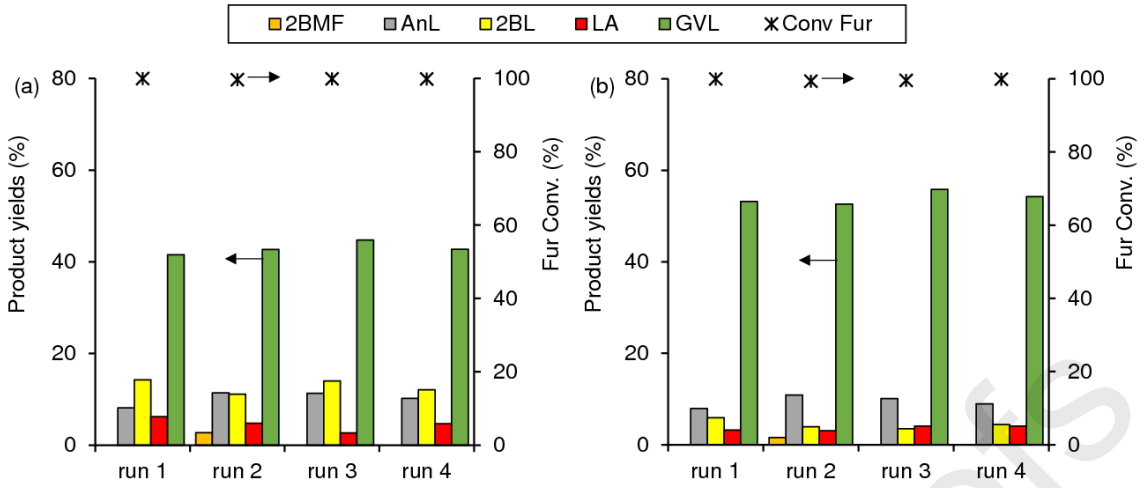

Fig. 10. Catalyst stability of Hf-deAlbeta-n (a) and Hf-WdeSAlBeta-m (b) in the reaction of Fur/2BuOH, at 180 ºC (24 h): Fur conversion (*) and bioproduct yields (bars).

4. Conclusions

In this work, the first Hf-containing BEA material possessing an intracrystalline hierarchical pore system, was prepared by using a top-down strategy. This material promoted different integrated reaction routes leading to the versatile bioproduct γ-valerolactone (GVL). GVL yields of up to 99 %, 91 % and 53 % were reached for the increasingly integrated and demanding reactions of levulinic acid (LA), α-angelica lactone (AnL) and furfural (Fur), respectively, at 180 °C (24 h). Hf-WdeSAlBeta-m performed better than nanocrystalline hafnium- or zirconium-containing Beta zeolites prepared via post-synthesis dealumination of commercial nanocrystalline H-Beta-m and solid-state impregnation (SSI) and calcination of a M precursor (giving M-deAlBeta-n). The superior catalytic performance of the hierarchical catalyst Hf-WdeSAlBeta-m correlated with its higher amount of total acid sites (and L/B ratio) and considerably enhanced mesoporous specific surface area. Studies of the influence of the reaction temperature (150 and 180 °C) and type of H-donor agent indicated that GVL formation was enhanced using 2-butanol at 180 °C. An overall reaction mechanism was proposed, and a kinetic model was developed which fitted reasonably well the experimental data for the integrated conversion of Fur to GVL, in the presence of Hf-deAlBeta-n or Hf-WdeSAlBeta-m. Molecular level characterization and catalytic tests of the materials suggested that the M-sites acted as Lewis acid sites in catalytic transfer hydrogenation (CTH) steps, and the Brønsted acidity may promote steps such as ring-opening of furanic

intermediates to LA and levulinate esters. The multifunctional materials were stable heterogeneous catalysts and their textural, acid, structural and morphological properties were essentially preserved.

It may be advantageous to consider changing the transition metal from, for example, typically used tin or zirconium to hafnium in the development of heterogeneous catalysts for Fur to GVL. On the other hand, it is envisaged that crystalline microporous Hf-containing zeolites possessing different structures and morphologies may be effective multifunctional stable catalysts for different acid-CTH reaction systems, and their properties may be tuned by varying, for example, the Hf content, Si/Al ratio and texture to meet superior performances for the desired reactions.

Acknowledgements

This work was developed within the scope of the project CICECO-Aveiro Institute of Materials, UIDB/50011/2020 & UIDP/50011/2020, financed by national funds through the Portuguese Foundation for Science and Technology/MCTES. The positions held by M.M.A. and A.F.S. were funded by national funds (OE), through FCT, I.P., in the scope of the framework contract foreseen in the numbers 4, 5 and 6 of article 23 of the Decree-Law 57/2016 of 29 August, changed by Law 57/2017 of 19 July. The position held by A.F.S. was funded by Project POCI-01-0145-FEDER-030075 (COMPETE 2020 Operational Thematic Program for Competitiveness and Internationalization) co-financed by national funds through the FCT/MCTES and the European Union through the European Regional Development Fund under the Portugal 2020 Partnership Agreement. The NMR spectrometer used is part of the National NMR Network (PTNMR) and is partially supported by Infrastructure Project Nº 022161 (co-financed by FEDER through COMPETE 2020, POCI and PORL and FCT through PIDDAC). The authors are grateful to Dr Gonzalo Otero Irurueta from TEMA (University of Aveiro) for the helpful discussions of the XPS spectroscopy results.

References

[1] Food and Agriculture Organization of the United Nations (FAO), in: ISBN 978-92-5-106653-9 (Ed.), What woodfuels can do to mitigate climate change? Rome, Italy, 2010, p.162. Data accessed: 17 June 2021, http://www.fao.org/3/i1756e/i1756e00.htm.

[2] L. Gustavsson, J. Holmberg, V. Dornburg, R. Sathre, T. Eggers, K. Mahapatra, G. Marland, Energ. Policy 35 (2007) 5671.

[3] J. Sherwood, Bioresource Technol. 300 (2020) 122755.

[4] R. Salvador, F. N. Puglieri, A. Halog, F.G. de Andrade, C. M. Piekarski, A. C. de Francisco, J. Clean. Prod. 278 (2021) 124341.

[5] H. S. Al-Battashi, N. Annamalai, N. Sivakumar, S. Al-Bahry, B. N. Tripathi, Q. D. Nguyen, V. K. Gupta, Rev. Environ. Sci. Bio. 18 (2019) 183.

[6] M. Kircher, New Biotechnol. 60 (2021) 96.

[7] P. Zhou, Z. Zhang, Catal. Sci. Technol. 6 (2016) 3694.

[8] X. Luo, Y. Li, N. K. Gupta, B. Sels, J. Ralph, L. Shuai, Angew. Chem. Int. Ed. 59 (2020) 11704.

[9] A. Deneyer, T. Ennaert, B. F. Sels, Curr. Opin. Green Sustain. Chem. 10 (2018) 11.

[10] International Furan Chemicals (IFC), Applications of Furfural, 2016. Data accessed: 17 June 2021, http://www.furan.com/furfural_applications_of_furfural.html.

[11] International Furan Chemicals (IFC), Furfuryl alcohol, 2016. Data accessed: 17 June 2021, http://www.furan.com/furfuryl_alcohol.html.

[12] R. Mariscal, P. Maireles-Torres, M. Ojeda, I. Sádaba, M. López Granados, Energ. Environ. Sci. 9 (2016) 1144.

[13] Y. Wang, D. Zhao, D. Rodríguez-Padrón, C. Len, Catalysts 9 (2019) 796.

[14] Y. Nakagawa, M. Tamura, K. Tomishige, ACS Catal. 3 (2013) 2655.

[15] Grand View Research (GVR), Furfuryl alcohol market size, share and trends analysis report by application (resins, solvent, corrosion inhibitor), by end use (foundry, agriculture), by region, and segment forecasts, 2020-2027, 2020, p. 90. Data accessed: 17 June 2021, https://www.grandviewresearch.com/industry-analysis/furfuryl-alcohol-market.

[16] P. S. Watson, J. A. Nuzum, D. B. Rohr, D. E. Newquist, C. T. Crawford, L. M. Bragg, Furfuryl alcohol from China, South Africa, and Thailand, U. S. International Trade Commission, Washing DC, 1994, p. 72.

[17] K. Yan, G. Wu, T. Lafleur, C. Jarvis, Renew. Sust. Energ. Rev. 38 (2014) 663.

[18] R. Xu, K. Liu, H. Du, H. Liu, X. Cao, X. Zhao, G. Qu, X. Li, B. Li, C. Si, ChemSusChem 13 (2020) 6461.

[19] L. Ye, Y. Han, J. Feng, X. Lu, Ind. Crop. Prod. 144 (2020) 112031.

[20] H. P. Winoto, B. S. Ahn, J. Jae, J. Ind. Eng. Chem. 40 (2016) 62.

[21] H. P. Winoto, Z. A. Fikri, J.-M. Ha, Y.-K. Park, H. Lee, D.J. Suh, J. Jae, Appl. Catal. B: Environ. 241 (2019) 588.

[22] M. J. Climent, A. Corma, S. Iborra, Green Chem. 16 (2014) 516.

[23] X. Tang, X. Zeng, Z. Li, L. Hu, Y. Sun, S. Liu, T. Lei, L. Lin, Renew. Sust. Energ. Rev. 40 (2014) 608.

[24] K. Yan, Y. Yang, J. Chai, Y. Lu, Appl. Catal. B: Environ. 179 (2015) 292.

[25] Decision Databases, Global gamma valerolactone (CAS 108-29-2) market 2020 by manufacturers, regions, type and application, forecast to 2025, 2020. Data accessed: 17 June 2021, https://www.decisiondatabases.com/ip/29885-gamma-valerolactone-market-analysis-report.

[26] BCFocus, Global gamma valerolactone (CAS 108-29-2) market 2020 analysis, types, applications, forecast and Covid-19 impact analysis, 2020. Data accessed: 17 June 2021, https://bcfocus.com/global-gamma-valerolactone-cas-108-29-2-market-2020-analysis-types-applications-forecast-and-covid-19-impact-analysis-2025/.

[27] L. E. Manzer, Appl. Catal. A: Gen. 272 (2004) 249.

[28] I. T. Horváth, Green Chem. 10 (2008) 1024.

[29] A. Bohre, S. Dutta, B. Saha, M. M. Abu-Omar, ACS Sustain. Chem. Eng. 3 (2015) 1263.

[30] K. L. Á. Bereczky, M. Farkas, S. Dóbé, Natural Resources 5 (2014) 177.

[31] I. T. Horváth, H. Mehdi, V. Fábos, L. Boda, L. T. Mika, Green Chem. 10 (2008) 238.

[32] T. Werpy, G. Petersen, in: US Department of Energy (Ed.), Top Value Added Chemicals from Biomass: Volume I - Results of Screening for Potential Candidates from Sugars and Synthesis Gas, National Renewable Energy Lab., Golden, CO (US), 2004, p.76. Data accessed: 17 June 2021, https://www.osti.gov/servlets/purl/15008859.

[33] J. J. Bozell, G.R. Petersen, Green Chem. 12 (2010) 539.

[34] L.E. Manzer, in: ACS Symposium Series, Chapter 4: Biomass derivatives: A sustainable source of chemicals in Feedstocks for the Future, American Chemical Society, vol. 921, 2006, pp. 40.

[35] Z. Yu, X. Lu, J. Xiong, X. Li, H. Bai, N. Ji, ChemSusChem 13 (2020) 2916.

[36] R. Weng, Z. Yu, J. Xiong, X. Lu, Green Chem. 22 (2020) 3013.

[37] S. Dutta, I. K. M. Yu, D. C. W. Tsang, Y. H. Ng, Y. S. Ok, J. Sherwood, J. H. Clark, Chem. Eng. J. 372 (2019) 992.

[38] A. Shivhare, A. Kumar, R. Srivastava, ChemCatChem 13 (2021) 59.

[39] X. Jin, B. Yin, Q. Xia, T. Fang, J. Shen, L. Kuang, C. Yang, ChemSusChem 12 (2019) 71.

[40] M. J. Gilkey, B. Xu, ACS Catal. 6 (2016) 1420.

[41] W. Fang, A. Riisager, Green Chem. 23 (2021) 670.

[42] M. Chia, J. A. Dumesic, Chem. Commun. 47 (2011) 12233.

[43] Z. Yu, X. Lu, C. Liu, Y. Han, N. Ji, Renew. Sust. Energ. Rev. 112 (2019) 140.

[44] J. A. Melero, G. Morales, J. Iglesias, M. Paniagua, C. López-Aguado, K. Wilson, A. Osatiashtiani, Green Chem. 19 (2017) 5114.

[45] B. Hernández, J. Iglesias, G. Morales, M. Paniagua, C. López-Aguado, J. L. García Fierro, P. Wolf, I. Hermans, J. A. Melero, Green Chem. 18 (2016) 5777.

[46] C. López-Aguado, M. Paniagua, J. Iglesias, G. Morales, J. L. García-Fierro, J. A. Melero, Catal. Today 304 (2018) 80.

[47] M. Wang, L. Peng, X. Gao, L. He, J. Zhang, Sustain. Energ. Fuel. 4 (2020) 1383.

[48] S. Song, L. Di, G. Wu, W. Dai, N. Guan, L. Li, Appl. Catal. B: Environ. 205 (2017) 393.

[49] C. López-Aguado, M. Paniagua, J. A. Melero, J. Iglesias, P. Juárez, M. L. Granados, G. Morales, Catalysts 10 (2020) 678.

[50] L. Ye, Y. Han, H. Bai, X. Lu, ACS Sustain. Chem. Eng. 8 (2020) 7403.

[51] B. Srinivasa Rao, P. Krishna Kumari, P. Koley, J. Tardio, N. Lingaiah, Mol. Catal. 466 (2019) 52.

[52] T. Zhang, Y. Lu, W. Li, M. Su, T. Yang, A. Ogunbiyi, Y. Jin, Int. J. Hydrogen Energ. 44 (2019) 14527.

[53] H. Zhang, W. Yang, I.I. Roslan, S. Jaenicke, G.-K. Chuah, J. Catal. 375 (2019) 56.

[54] L. Bui, H. Luo, W.R. Gunther, Y. Román-Leshkov, Angew. Chem. Int. Ed. 52 (2013) 8022.

[55] M. M. Antunes, S. Lima, P. Neves, A. L. Magalhães, E. Fazio, F. Neri, M. T. Pereira, A. F. Silva, C. M. Silva, S. M. Rocha, M. Pillinger, A. Urakawa, A. A. Valente, Appl. Catal. B: Environ. 182 (2016) 485.

[56] S. Rojas-Buzo, P. García-García, A. Corma, ChemSusChem 11 (2018) 432.

[57] M. Koehle, R. F. Lobo, Catal. Sci. Technol. 6 (2016) 3018.

[58] H.Y. Luo, D. F. Consoli, W. R. Gunther, Y. Román-Leshkov, J. Catal. 320 (2014) 198.

[59] B. Tang, S. Li, W.-C. Song, E.-C. Yang, X.-J. Zhao, N. Guan, L. Li, ACS Sustain. Chem. Eng. 7 (2019) 16329.

[60] W. Li, Z. Cai, H. Li, Y. Shen, Y. Zhu, H. Li, X. Zhang, F. Wang, Mol. Catal. 472 (2019) 17.

[61] M. M. Antunes, P. Neves, A. Fernandes, S. Lima, A. F. Silva, M. F. Ribeiro, C. M. Silva, M. Pillinger, A. A. Valente, Catal. Sci. Technol. 6 (2016) 7812.

[62] M. M. Antunes, S. Lima, P. Neves, A. L. Magalhães, E. Fazio, A. Fernandes, F. Neri, C. M. Silva, S. M. Rocha, M. F. Ribeiro, M. Pillinger, A. Urakawa, A. A. Valente, J. Catal. 329 (2015) 522.

[63] Y. Wang, J. D. Lewis, Y. Román-Leshkov, ACS Catal. 6 (2016) 2739.

[64] B. Tang, W. Dai, X. Sun, G. Wu, N. Guan, M. Hunger, L. Li, Green Chem. 17 (2015) 1744.

[65] C. A. Emeis, J. Catal. 141 (1993) 347.

[66] A. Simon-Masseron, J. P. Marques, J. M. Lopes, F. R. Ribeiro, I. Gener, M. Guisnet, Appl. Catal. A: Gen. 316 (2007) 75.

[67] O. Mangla, S. Roy, Proceedings 3 (2019) 10.

[68] S.J. Gregg, K.S.W. Sing, Adsorption, surface area and porosity, Academic Press, London, UK, 1982.

[69] M. Thommes, Chem. Ing. Tech. 82 (2010) 1059.

[70] C. Schlumberger, M. Thommes, Adv. Mater. Interfaces 8 (2021) 2002181.

[71] J. Pérez-Ramírez, C.H. Christensen, K. Egeblad, C. H. Christensen, J. C. Groen, Chem. Soc. Rev. 37 (2008) 2530.

[72] V. A. Gritsenko, T. V. Perevalov, D. R. Islamov, Phys. Rep. 613 (2016) 1.

[73] S. Lee, D.-J. Yun, S.-W. Rhee, K. Yong, J. Mater. Chem. 19 (2009) 6857.

[74] Y.-B. Huang, Y.-J. Luo, F. Wang, Nanomaterials 9 (2019) 1128.

[75] Y. Zhu, G. Chuah, S. Jaenicke, J. Catal. 227 (2004) 1.

[76] L. Gao, G. Li, Z. Sheng, Y. Tang, Y. Zhang, J. Catal. 389 (2020) 623.

[77] G. Yang, L. Wang, H. Jiang, React. Chem. Eng. 5 (2020) 1833.

[78] P. Zhao, W. Qian, H. Ma, H. Sheng, H. Zhang, W. Ying, Catal. Lett. 151 (2021) 940.

[79] A. Ramanathan, H. Zhu, R. Maheswari, B. Subramaniam, Chem. Eng. J. 278 (2015) 113.

[80] A. Ramanathan, M. C. Castro Villalobos, C. Kwakernaak, S. Telalovic, U. Hanefeld, Chemistry 14 (2008) 961.

[81] A. Ramanathan, D. Klomp, J.A. Peters, U. Hanefeld, J. Mol. Catal. A: Chem. 260 (2006) 62

[82] X. Li, X. Yuan, G. Xia, J. Liang, C. Liu, Z. Wang, W. Yang, J. Catal. 392 (2020) 175.

[83] L. Armelao, C. Eisenmenger-Sittner, M. Groenewolt, S. Gross, C. Sada, U. Schubert, E. Tondello, A. Zattin, J. Mater. Chem. 15 (2005) 1838.

[84] J. Kim, K. Yong, J. Appl. Phys. 100 (2006) 044106.

[85] S. Telalović, A. Ramanathan, J. F. Ng, R. Maheswari, C. Kwakernaak, F. Soulimani, H. C. Brouwer, G. K. Chuah, B. M. Weckhuysen, U. Hanefeld, Chemistry 17 (2011) 2077.

[86] A. Rodríguez-Fernández, J. R. Di Iorio, C. Paris, M. Boronat, A. Corma, Y. Román-Leshkov, M. Moliner, Chem. Sci. 11 (2020) 10225.

[87] V. L. Sushkevich, A. Vimont, A. Travert, I. I. Ivanova, J. Phys. Chem. C 119 (2015) 17633.

[88] G. Yang, L. Zhou, Sci. Rep. 7 (2017) 16113.

[89] M. M. Antunes, D. Falcão, A. Fernandes, F. Ribeiro, M. Pillinger, J. Rocha, A. A. Valente, Catal. Today 362 (2021) 162.

[90] L. Mafra, J. A. Vidal-Moya, T. Blasco, in: G.A. Webb (Ed.), Chapter 4: Structural Characterization of Zeolites by Advances Solid State NMR Spectroscopic Methods, Annual Reports on NMR Spectroscopy, Academic Press, cidade, 2012, pp. 259.

[91] J. Zheng, M. Wu, F. Jiang, W. Su, M. Hong, Chem. Sci. 6 (2015) 3466.

[92] S. Rojas-Buzo, B. Bohigues, C.W. Lopes, D. M. Meira, M. Boronat, M. Moliner, A. Corma, Chem. Sci. 12 (2021) 10106.

[93] M. Ravi, V. L. Sushkevich, J. A. van Bokhoven, Nat. Mater. 19 (2020) 1047.

[94] A. J. Marchi, G. F. Froment, Appl. Catal. 71 (1991) 139.

[95] R. T. J. Gerards, A. Fernandes, I. Graça, M. F. Ribeiro, Fuel 260 (2020) 116372.

[96] J. A. Melero, G. Morales, J. Iglesias, M. Paniagua, C. López-Aguado, Ind. Eng. Chem. Res. 57 (2018) 11592.

[97] Y. Lu, W. Li, Y. Zhu, T. Zhang, Q. Zhang, Q. Liu, BioResources 13 (2018) 5925.

[98] K. D. Kim, J. Kim, W. Y. Teoh, J.-C. Kim, J. Huang, R. Ryoo, RSC Adv. 10 (2020) 35318.

[99] Y. Kuwahara, H. Kango, H. Yamashita, ACS Sustain. Chem. Eng. 5 (2017) 1141.

[100] G. Morales, J. A. Melero, J. Iglesias, M. Paniagua, C. López-Aguado, React. Chem. Eng. 4 (2019) 1834.

[101] J. Iglesias, J. A. Melero, G. Morales, M. Paniagua, B. Hernández, A. Osatiashtiani, A. F. Lee, K. Wilson, Catal. Sci. Technol. 8 (2018) 4485.

[102] J. He, H. Li, Y. Xu, S. Yang, Renew. Energ. 146 (2020) 359.

[103] K. Y. Nandiwale, M. Vishwakarma, S. Rathod, I. Simakova, V. V. Bokade, Energ. Fuel. 35 (2021) 539.

[104] S. Gundekari, K. Srinivasan, Catal. Lett. 149 (2019) 215.

[105] V. B. Khajone, S. U. Raut, S. A. Deshmukh, K. J. Bhansali, K. R. Balinge, P. N. Muskawar, P. R. Bhagat, Biomass Conversion and Biorefinery (2021) https://doi.org/10.1007/s13399-13021-01688-13393.

[106] Y. Xie, F. Li, J. Wang, R. Wang, H. Wang, X. Liu, Y. Xia, Mol. Catal. 442 (2017) 107.

[107] C. Xie, J. Song, B. Zhou, J. Hu, Z. Zhang, P. Zhang, Z. Jiang, B. Han, ACS Sustain. Chem. Eng. 4 (2016) 6231.

[108] X. Tang, H. Chen, L. Hu, W. Hao, Y. Sun, X. Zeng, L. Lin, S. Liu, Appl. Catal. B: Environ. 147 (2014) 827.

[109] W. Gong, C. Chen, R. Fan, H. Zhang, G. Wang, H. Zhao, Fuel 231 (2018) 165.

[110] J. P. C. Pereira, W. Overbeek, N. Gudiño-Reyes, E. Andrés-García, F. Kapteijn, L. A. M. van der Wielen, A. J. J. Straathof, Ind.Eng. Chem. Res. 58 (2019) 296.

[111] S. M. Scully, J. Orlygsson, in: M. Hosseini (Ed.), Advanced Bioprocessing for Alternative Fuels, Biobased Chemicals, and Bioproducts, Woodhead Publishing, 2019, pp. 83.

[112] H. C. Rothlis, US Patent US4609624A (1986), to Les Services de Consultation D. B. Plus Limitee.

[113] M.E. Davis, Nature 417 (2002) 813.

[114] T. Prasomsri, W. Jiao, S. Z. Weng, J. G. Martinez, Chem. Commun. 51 (2015) 8900.

[115] S. Zhu, Y. Xue, J. Guo, Y. Cen, J. Wang, W. Fan, ACS Catal. 6 (2016) 2035.

[116] Q. Peng, H. Wang, Y. Xia, X. Liu, Appl. Catal. A: General 621 (2021) 118203.

[117] L. Peng, X. Gao, Y. Liu, J. Zhang, L. He, Energ. Fuel. 35 (2021) 4182.

[118] J. Han, J. Cho, J.-C. Kim, R. Ryoo, ACS Catal. 8 (2018) 876.

[119] M. Paniagua, J.A. Melero, J. Iglesias, G. Morales, B. Hernández, C. López-Aguado, Appl. Catal. A: Gen. 537 (2017) 74.

[120] X. Yufei, Z. Heng, L. Hu, Y. Song, Current Green Chem. 7 (2020) 304.

[121] A. Seretis, P. Diamantopoulou, I. Thanou, P. Tzevelekidis, C. Fakas, P. Lilas, G. Papadogianakis, Front. Chem. 8 (2020), doi: 10.3389/fchem.2020.00221.

[122] P. Vasanthakumar, R. Karvembu, ACS Sustain. Chem. Eng. 8 (2020) 17069.

[123] I. Obregón, I. Gandarias, M. G. Al-Shaal, C. Mevissen, P. L. Arias, R. Palkovits, ChemSusChem 9 (2016) 2488.

[124] K. Sakakibara, K. Endo, T. Osawa, Catal. Commun. 125 (2019) 52.

[125] J. Gu, J. Zhang, Y. Wang, D. Li, H. Huang, H. Yuan, Y. Chen, Ind. Crop. Prod. 145 (2020) 112133.

[126] C.-Y. Hsiao, H.-Y. Chiu, T.-Y. Lin, K.-Y.A. Lin, Chem. Eng. Commun. (2020) 1511, doi: 10.1080/00986445.2020.1791833.

[127] W.-C. Yun, T.-Y. Lin, H.-Y. Chiu, K.-Y.A. Lin, Waste Biomass Valori. 11 (2020) 2783.

[128] M. G. Al-Shaal, M. Calin, I. Delidovich, R. Palkovits, Catal. Commun. 75 (2016) 65.

[129] A. S. Amarasekara, M. A. Hasan, Catal. Commun. 60 (2015) 5

[130] X. Li, Z. Du, Y. Wu, Y. Zhen, R. Shao, B. Li, C. Chen, Q. Liu, H. Zhou, RSC Adv. 10 (2020) 9985.

[131] P. K. Jori, V.H. Jadhav, Catal. Lett. 150 (2020) 2038.

[132] W.-C. Yun, M.-T. Yang, K.-Y.A. Lin, J. Colloid Interf. Sci. 543 (2019) 52.

[133] T.-Y. Lin, K.-Y.A. Lin, J. Taiwan Inst. Chem. E. 96 (2019) 321.

[134] Z. Xue, J. Jiang, G. Li, W. Zhao, J. Wang, T. Mu, Catal. Sci. Technol. 6 (2016) 5374.

[135] J. Wang, S. Jaenicke, G.-K. Chuah, RSC Adv 4 (2014) 13481.

[136] A. Kumar, R. Srivastava, Sustain. Energy Fuels 3 (2019) 2475.

Declaration of interests

☒ The authors declare that they have no known competing financial interests or personal relationships that could have appeared to influence the work reported in this paper.

☐The authors declare the following financial interests/personal relationships which may be considered as potential competing interests:

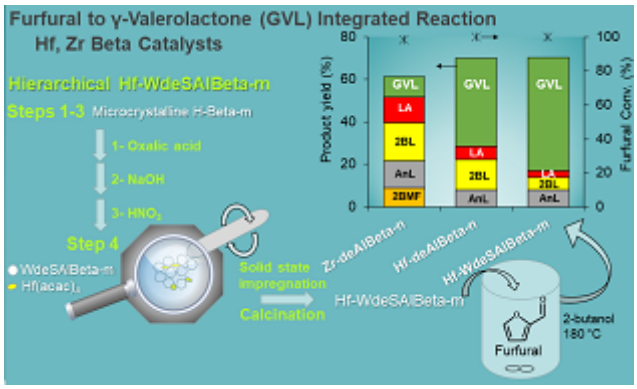

Highlights

Integrated γ-valerolactone production from furfural, angelica lactone, levulinic acid

Nanocrystalline hafnium-Beta (Hf-deAlBeta-n) was superior to the zirconium analogue

First intracrystalline hierarchical Hf-containing BEA zeotype (Hf-WdeSAlBeta-m)

Hf-WdeSAlBeta-m performed superiorly to Hf-deAlBeta-n for integrated reactions

Hf-WdeSAlBeta-m possessed enhanced acidity and mesopore area, favouring activity